Design, Fabrication, and Testing of a Three-Dimensional, Plastically-Deformed, Monolithic Compliant HexFlex Nanomanipulator

by

Samuel N. Korb

SUBMITTED TO THE DEPARTMENT OF MECHANICAL ENGINEERING IN PARTIAL FULFILLMENT OF THE REQUIREMENTS FOR THE DEGREE OF

BACHELOR OF SCIENCE

AT THE

MASSACHUSETTS INSTITUTE O F TECHNOLOGY

JUNE 2004

Signature of Author: .....
Department of Mechanical Engineering
May 7, 2004

Certified by: .....
Martin L. Culpepper III
Rockwell International Assistant Professor of Mechanical Engineering
Thesis Supervisor

Accepted by: .....
Ernest G. Cravalho
Professor of Mechanical Engineering
Chairman, Undergraduate Thesis Committee

Design, Fabrication, and Testing of a Three-Dimensional, Plastically-Deformed, Monolithic Compliant HexFlex Nanomanipulator

by

Samuel N. Korb

Submitted to the Department of Mechanical Engineering
on May 7, 2004 in Partial Fulfillment of the
Requirements for the Degree of Bachelor of Science in
Mechanical Engineering

ABSTRACT

An experimental study was performed to investigate the possibility of incorporating plastic deformation into a precision compliant mechanism design. The particular application of a compliant HexFlex Nanomanipulator was chosen as a mechanism to extend plastically into three dimensions. The mechanism was built to competitive Nanomanipulator functional requirements employing non-precision methods of fabrication, such as the abrasive waterjet. New tooling was created in order to selectively define which parts of the delicate mechanism to plastically deform.

Once formed, the mechanism was tested to determine if the plastic deformation process in the forming of the mechanism has undesirable effects on its performance as a Nanomanipulator. An input/output correlation test was performed in order to determine the correspondence of the physical model to a finite-element analysis of the same. The out-of-plane, time variable position drift (both immediately after forming as well as a week after forming) was measured to quantify the effects of creep and stress relaxation on Nanomanipulator position. The out-of-plane creep under near-yield loading conditions was also measured.

For the work volume of 75x75x75 μm^3, the experimental results corresponded to within 8%, on average, to the predicted values. Over the course of the 24 hours following the plastic deformation, the output stage drifted 6 μm due to stress relaxation, compared with a daily fluctuation due to thermal expansion and contraction of amplitude 1 μm. Over the course of 24 hours of loading the mechanism near its elastic yield point, the mechanism crept 2 μm.

Thesis Supervisor: Martin L. Culpepper III
Title: Rockwell International Assistant Professor of Mechanical Engineering

Table of Contents

1.0 Introduction

Traditional methodologies of machine design involve rigid elements connected with joints to enable relative motion between machine components and thereby introduce the desired degrees of freedom. An example of a mechanism designed using these conventions appears in Figure 1.

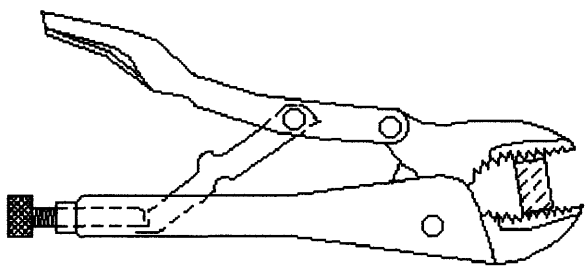

Image courtesy of Larry Howell

Figure 1: Vise-grip Traditionally-designed Mechanism

This Vise-grip is a four-bar mechanism, with the different components, fabricated from a steel or otherwise stiff metal, hinging at pin joints. An input motion at the left side of pinching the handles is transferred through the linkage to the output motion of the jaws closing on the block.

Compliant mechanisms take a different approach to mechanism design. The mechanism, often fabricated from one piece of material, takes advantages of the elastic properties that all materials exhibit to introduce degrees of freedom. An example of a compliant approach to the gripper pictured in Figure 1 appears in Figure 2.

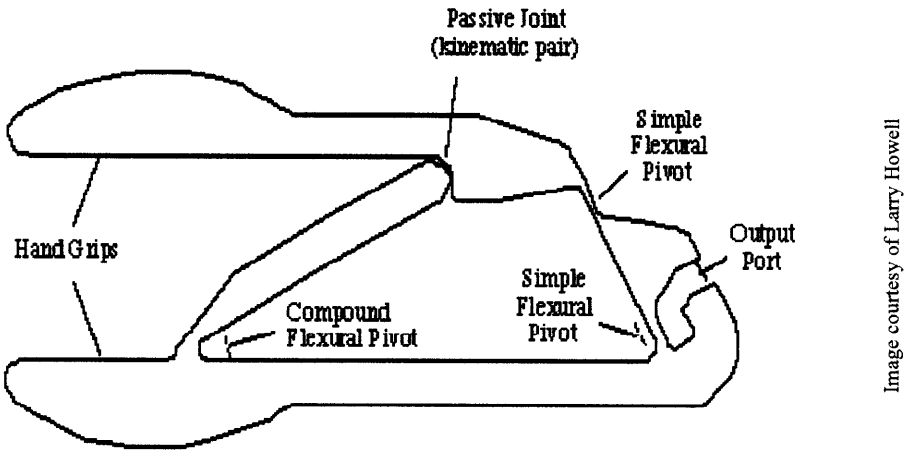

Figure 2: Compliant-designed Mechanism

In this case, the same four-bar linkage approach is evident, but instead of sliding pivots, the mechanism's material is tapered at those points, reducing its resistance to bending, thus creating a pivot made of continuous material.

The primary reason for using compliant mechanisms is ease of assembly and lack of hysteresis. When a compliant design replaces two bars and the pivot between them with one continuous piece of material, the number of parts to be assembled drops from three to one. Fixturing issues, time costs, assembly, tolerances and specialization of labor are all reduced. Hysteresis is reduced, as well; whenever to parts are brought together, and they must slip relative to one another, there must be some small gap between them to introduce the freedom necessary to move. This small amount of space can lead to a lack of correlation between input and output in the regime when load conditions are altered, and the parts move across the gaps. Friction at these interfaces/joints is also a well-known source of hysteresis in mechanisms.

For most applications on a macro scale, the hysteresis due to the misfit between parts is acceptable, as it makes up a very small amount of the overall motion. However, when the

application is in the precision domain, with position resolution on the nanometer scale, the errors accumulate to a larger percentage of the intended accuracy and/or repeatability.

An example of the problems associated with scaling mechanisms down is in the case of a six degree of freedom hexapod. A common macroscopic application of this configuration is in flight simulators, as shown in Figure 3.

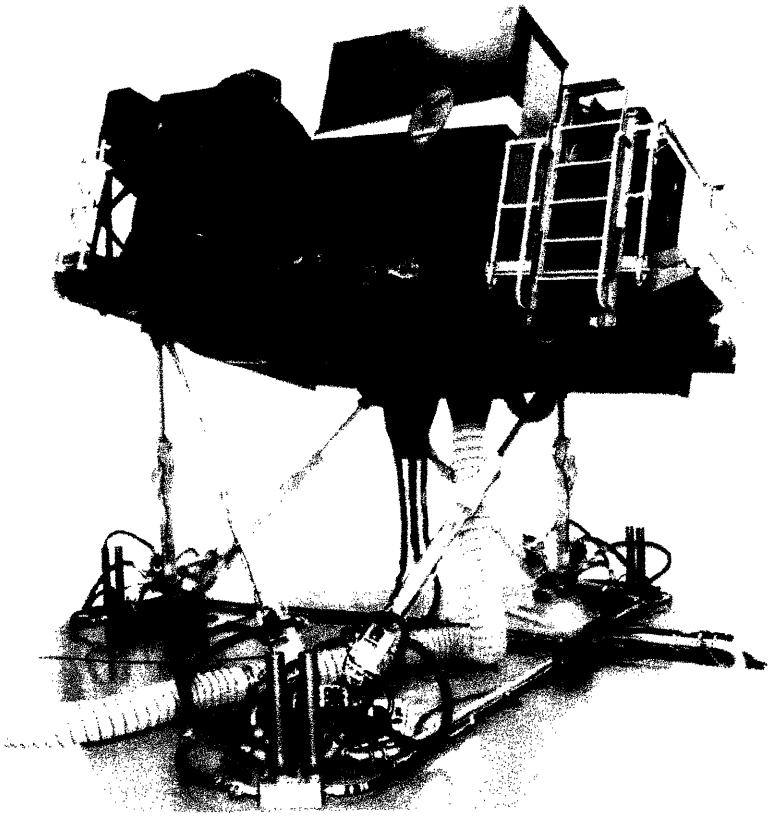

Image courtesy of CIMAR, Univ of FL

Figure 3: Flight Simulator Employing Hexapod Parallel Mechanism

Two rigid platforms, the ground and the simulator cabin, are separated by six linear actuator pistons. By varying the length of the pistons, it is possible to achieve six relative degrees of freedom between the two platforms. This is known as a Stewart-Gough Platform. This mechanism has been in use since the middle of the 19th century as a ubiquitous means of achieving six degree-of-freedom motion. At each of the many joints in this structure, there is a finite gap between the assembled joint components.

When this same technology is designed for use in nanometer-level positioning, the design varies little, except for increased precision (and cost) of the joints between parts. An example of such a Nanomanipulator is shown in Figure 4.

Image courtesy of Physik Instrumente

Figure 4: Nanomanipulator Employing a Stewart-Gough Platform

In recent years, a new approach to Nanomanipulation was developed at MIT's Precision Compliant Systems Design Laboratory. The mechanism, shown in Figure 5, is a monolithic compliant mechanism known as the HexFlex [1]. The mechanism operates based upon six compliant constraints which connect a stage (center triangle) to ground. Fundamentally, this design is different from a Hexapod or Stewart-Gough-Gough Platform in the application of compliant constraints (it is not simply a flattened Stewart-Gough platform) and the elimination of joints. The mechanism is normally operated in the elastic regime to achieve nanometer resolution movement in six degrees of freedom.

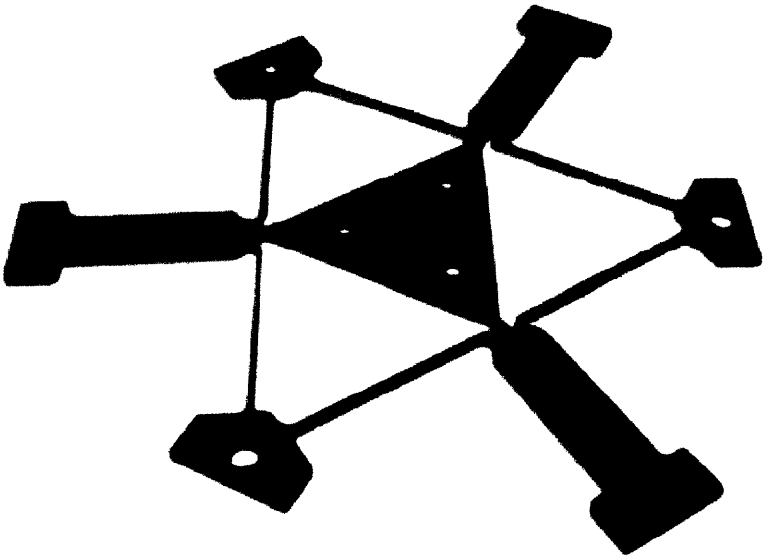

Image courtesy of Gordon Anderson

Figure 5: HexFlex Nanomanipulator

The mechanism was actuated at the ends of the three T-shaped tabs in two directions. The first was in-plane, pushing the tab in the plane of the mechanism parallel to the thin connecting beams. The second was out-of-plane, pushing the tab in a direction perpendicular to the plane of the mechanism. Actuating the three tabs in those two dimensions produced the six degrees of freedom at the output, on the center triangular stage. An embodiment of the mechanism integrated into a Nanomanipulator is shown in Figure 6.

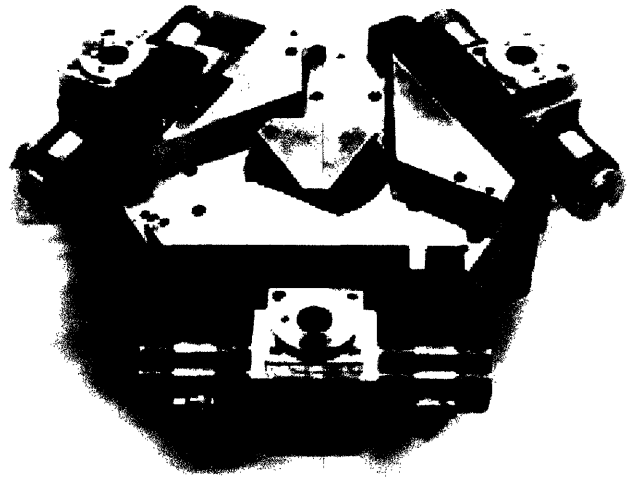

Image courtesy of Prof. Martin L. Culpepper

Figure 6: HexFlex Nanomanipulator system

One objective of the research was to investigate the potential for use of three-dimensional HexFlex mechanisms which are formed into a 3D shape from a 2D shape. This was to be done by plastically deforming a portion of a 2D mechanism out-of-plane to form a three dimensional geometry. Traditionally, precision engineers are taught that plastic deformation is to be avoided at all costs. Rough guidelines passed on via oral tradition, have been used to confine the deformation of precision flexures to less than 20% of the yield stress. However, through the course of a literature search, the author could find no concrete evidence, theoretical or experimental, to back up this guideline. As a result, another objective of this work was to investigate the degree of error which in introduced into a precision compliant mechanism due to plastic deformation prior to use. This work will provide the seed for future work in plastically deformed precision mechanisms.

Intuitively, we know that plastic deformation in many forms is not harmful to the function of a device. Plastic deformation is not uncommon to other manufacturing processes, as shown in Figure 7.

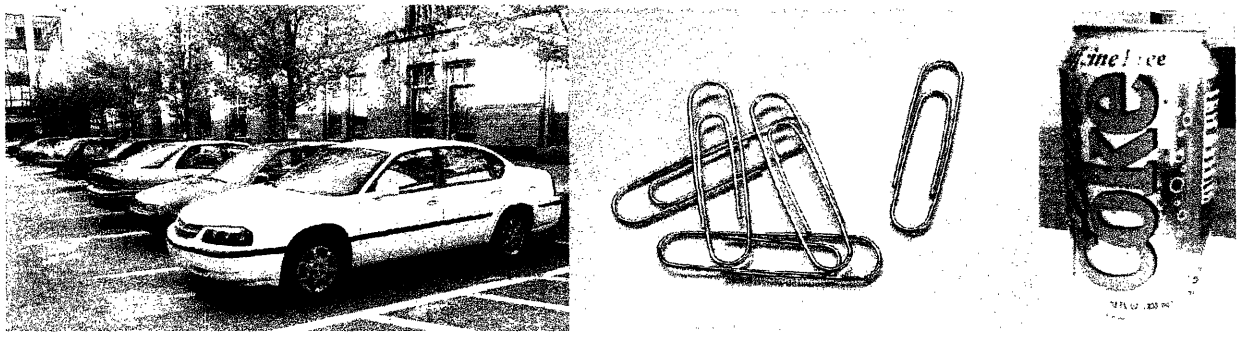

Image courtesy of Tom Fairbanks

Figure 7: Examples of Plastically Deformed Products

In the case of the car, the entire body is composed of sheet metal panels that have been plastically deformed in a stamping process. Paper clips begin as wire that is bent to shape. Soda cans start as circular discs of metal, and are drawn into cylinders. Thus, plastic deformation is not new to fabrication processes for machine elements or mechanisms. In addition, plastic deformation has been used extensively in sub-micron alignment and long-term fixation for laser alignment [2, 8, 9, 14] and photonics packaging [3, 5, 10, 11, 12, 15, 16]. However, in these cases, plastic deformation is employed in an iterative and "tweaking" process to achieve proper positioning, rather than guiding the deformations with intentionality.

However, given that plastic deformation is commonly used in fabrication processes, and that the operating regime is in the elastic domain, this mechanism should hypothetically be able to be created. Upon creation, testing should show the performance to conform to Finite-Element Analysis (FEA) models. It probably does not have any unpredictable effects due to post-processing stress relaxation during use that cannot be corrected by feedback mechanisms.

The success of the first objective (modeling 3D, plastically deformed mechanism) will be judged by the match between predictions from experimental results (after plastic deformation) and the pure elastic behavior predicted by FEA. The second objective (evaluation of time-variable error due to plastic deformation) is exploratory and therefore not subject to a binary evaluation criterion.

2.0 Functional Requirements

The functional requirements for the three dimensional HexFlex Nanomanipulator are guided by the potential applications, as well as existing capabilities of available conventional Nanomanipulators. A list of the latter appears in Table 1.

Table 1: Comparison Chart of Capabilities of Existing Nanomanipulators

Manufacturer	System Name	Work Volume [mm]	Linear Resolution [nm]	Angular Resolution [arc sec]	DOF
Physik Instrumente	F206	x(12),y(12),z(12)	33	0.4	6
Axsys	FAST 6 FIBER	x(25),y(06),z(50)	10	0.1	6
Axsys	FAST 30/300	x(25),y(06),z(50)	10	0.1	6
EXFO/burleigh	FR 1500 series	x(25),y(25),z(25)	0.1-20	0.1-4	6
EXFO/burleigh	FR 3000	x(25),y(25),z(25)	0.1-20	0.004-0.2	6
Elliot	MDE 881	x(40),y(25),z(06)	20	1	6
Elliot	NanoStage Six	x(28),y(28),z(10)	50	5	6
Melles Griot	NanoMax-HS	x(04),y(04),z(04)	30-1000	0.1-4	6
Aerotech	FiberMax	x(25),y(25),z(04)	2-10	0.03-0.06	6

The functional requirements for Nanomanipulators are guided largely by their intended applications. Nanomanipulators primarily function for precise alignment. In the original HexFlex project, the mechanism was used to guide a beam of light, through a strand of optical fiber. Optical applications such as this and also precise positioning of other optical elements, like mirrors or lenses, are well-suited to compliant mechanisms, as the force needed to actuate them is largely position-independent. Extreme accuracy in positioning is also necessary in the processing of silicon wafers, where the wafer must be correctly aligned with the mask before it is further treated.

The HexFlex mechanism achieved a working volume of 100 μm x 100 μm x 100 μm, with a resolution better than 5nm. While this resolution is on the scale of the other products, the range is noticeably smaller – about 10 to 100 times less than the compared products. This limitation is due to the fact that the HexFlex must maintain contiguity without lasting

deformation at all times. That is, it cannot move so far that it bends itself out of shape. This however is immaterial in many nano-scale applications as a range of several hundred microns is sufficient.

For the 3D version, the struts connecting the compliant pivots at the end of the tabs to the compliant pivots at the corners of the stage will likely deform elastically to some extent during loading. The energy absorbed in this bending process will not be transferred to the final output of the stage, so for approximately the same overall mechanism size, a reduction in operating range will likely be seen. Thus, the functional requirements for the operational volume will be 75 μm x 75 μm x 75 μm.

The mechanism will be a 3D monolithic compliant HexFlex Nanomanipulator. The initial forming process will be a two-dimensional non-precision process, and the part that emerges from that process must have reserves of metal incorporated into it that can be drawn on the secondary forming process to achieve the third dimension. The drawing process should be carefully set up so that only the desired regions of the mechanism are affected.

In order to facilitate testing of the mechanism, it must be able to interface with standard micrometer heads, in a way that minimizes hysteresis-inducing friction at the interface. There must also be a good interface for the measuring devices, both a dial gauge and a capacitance probe. For the dial gauge, there must be a patch of free surface at least the size of the dial gauge tip, which is approximately 0.08" in diameter. For the capacitance probe, there must be a smooth conducting surface that is greater than the area of the front of the capacitance probe, a circle 0.375" in diameter. The testing setup must sufficiently support the mechanism and the actuators and allow for adequate space to position the output sensors.

In addition, the total range of position drift due to this relaxation must be well below the total range of the mechanism. The same criteria must be true for creep effects at a loading condition near the yield stress for room-level temperatures.

3.0 Mechanism Design

In this section, the functional requirements for the mechanism and its support equipment will be presented.

3.1 Manipulator Design

In order to satisfy the functional requirement that the initial process be two-dimensional, the part was designed as a flat drawing that was extruded in the SolidWorks Computer-Aided Design (CAD) Package. An annotated drawing of the flat part appears in Figure 8. This was the file that was used to generate the machine code which drove the waterjet.

On this figure, Cartesian coordinate terminology is used to describe certain features (i.e. "Displacement in the y direction"), and in order to do this, a reference frame must be specified, as it has been on the Figure. The origin of the part is through its center, with z direction coming out of the page, y direction passing through the stub, and x direction normal to those two, in a right-handed reference frame.

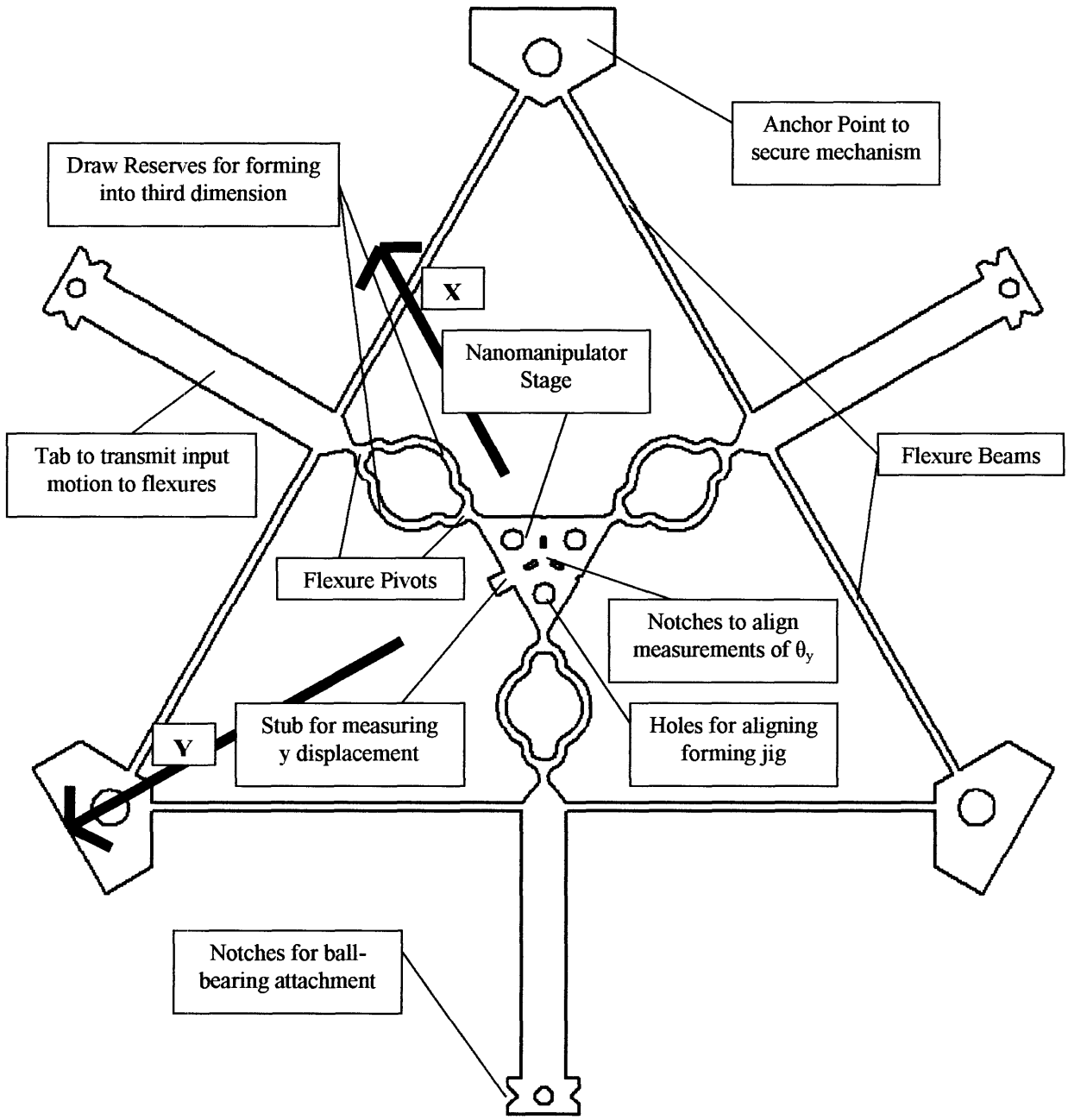

Figure 8: Annotated Drawing of 3D Nanomanipulator

This design incorporates many of the features and general size of the HexFlex in order to achieve many of the functional requirements relating to work volume. To secure the mechanism, the pentagonal plates at the edges are fitted with ¼" clearance holes. Attached to these are the long, thin flexure beams that introduce the ability for the tabs to pivot in-plane. The tabs are

fitted at the end with two notches and a small hole. These features will be where small ball bearings are glued, to act as the actual interface with the micrometer heads, thus minimizing the friction at the interface between the micrometer heads and the mechanism. The circular traces of the metal are the draw reserves. At either end of the draw reserves are the compliant pivots. To create these pivots, the material of the mechanism pinches in at these points. These pivots are the compliant equivalents of the ball joints at either end of the Stewart-Gough Platform pistons: the three tabs are displaced in two set input modes (in-plane and out-of-plane), and the pivots allow the center stage to come to the final output configuration. On the Stewart-Gough Platform, the six pistons are set to input lengths, and the ball pivots allow the stage to find the resultant output. The mechanism's stage has a few features which do not directly relate to the motion, but instead facilitate forming and measurement.

The mechanism is approximately the same overall size as the original HexFlex; the bolt holes for affixing the mechanism, and thus the vertices of the "large triangle," are 6" apart. The flexure beams are 1/16" thick, so that when the mechanism is cut out of 1/8" metal, the beams have a larger moment of inertia out-of-plane than in-plane. This reduces the propensity of the flexure beams to deflect downward when an out-of-plane input is applied, instead of pivoting around their axis to transmit the twist directly through. The tabs are 2" long from the center of the flexure beams to the center of the holes for the ball bearings.

The draw reserves were chosen to be curved beams because the process of beam bending was much easier to achieve than traditional deep drawing. The latter usually requires constant circumference of drawing, where as the HexFlex construction of this mechanism made that impossible, barring post-processing separation of the three different legs. However, this would have added another step to the production of the mechanism, and one that would have required

intricate milling or other three-dimensional cutting capability. In addition, deep drawing requires specialized machinery to control the drawing force and the force on the blank holder, not to mention a very uniform blank. These factors were undesirable for the functional requirement of fabricating this fairly intricate and delicate mechanism as simply and cheaply as possible. Beam bending, if the beams are properly isolated from the rest of the mechanism, though more complex than the simple one dimensional case, is fairly easy to accomplish, and is a much simpler plastic deformation process.

The material selected for the fabrication of the mechanism was 6061-T6 1/8" Aluminum. This was selected largely because of its availability and cost, while retaining the necessary requirements of good formability due to plastic behavior beyond the yield stress. Indeed, early versions of the HexFlex were formed from similar Aluminum, and in both cases, Aluminum proved adequate for the applications of this research because of its ability to be formed as well as operated in the correct regimes.

A view of the part that came out of the waterjet appears in Figure 9.

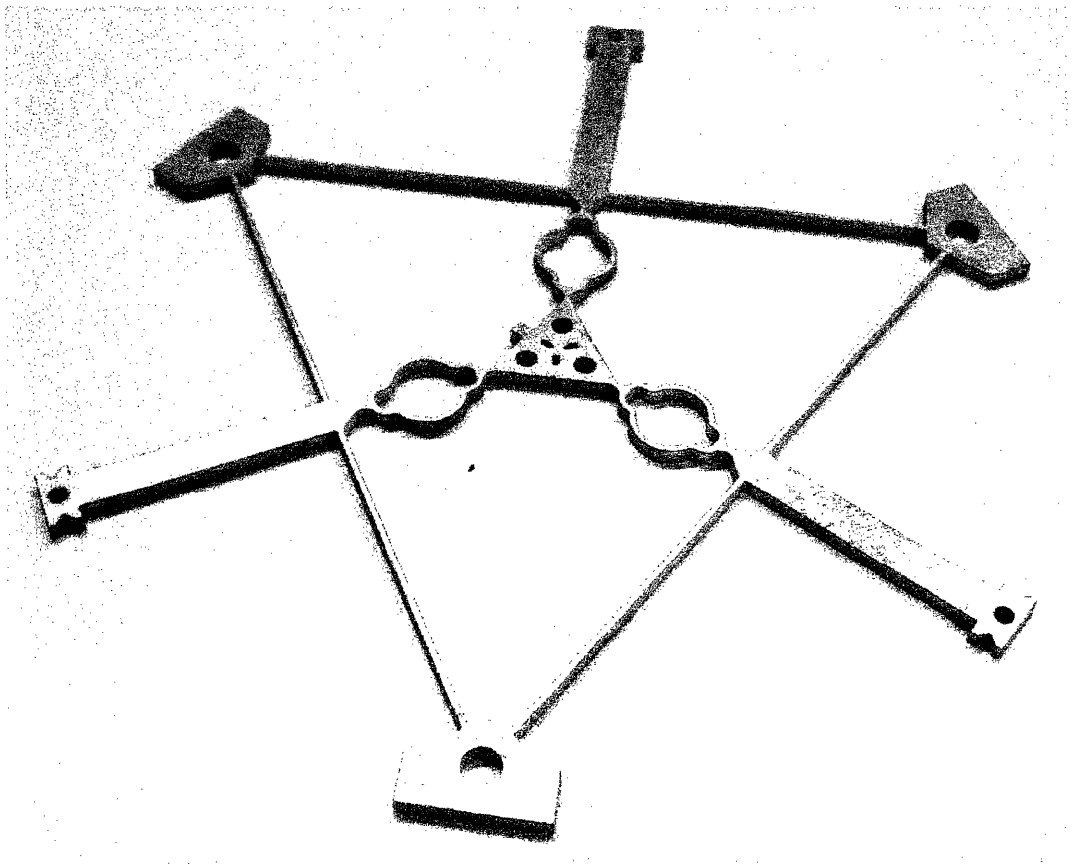

Figure 9: Mechanism after Waterjetting

3.2 Tooling Design

The functional requirement for the tooling was that it must plastically deform the mechanism in the correct places. The design parameters were two-fold: properly locate the mechanism, and then isolate the regions to be deformed so that deformation only occurs in the draw reserves. This is particularly critical because the draw reserves are adjacent to the compliant pivots. These pivots are the weakest part of the structure, and must not be exposed to the large stresses required to plastically deform the mechanism. The four main components of the tooling appear in Figure 10.

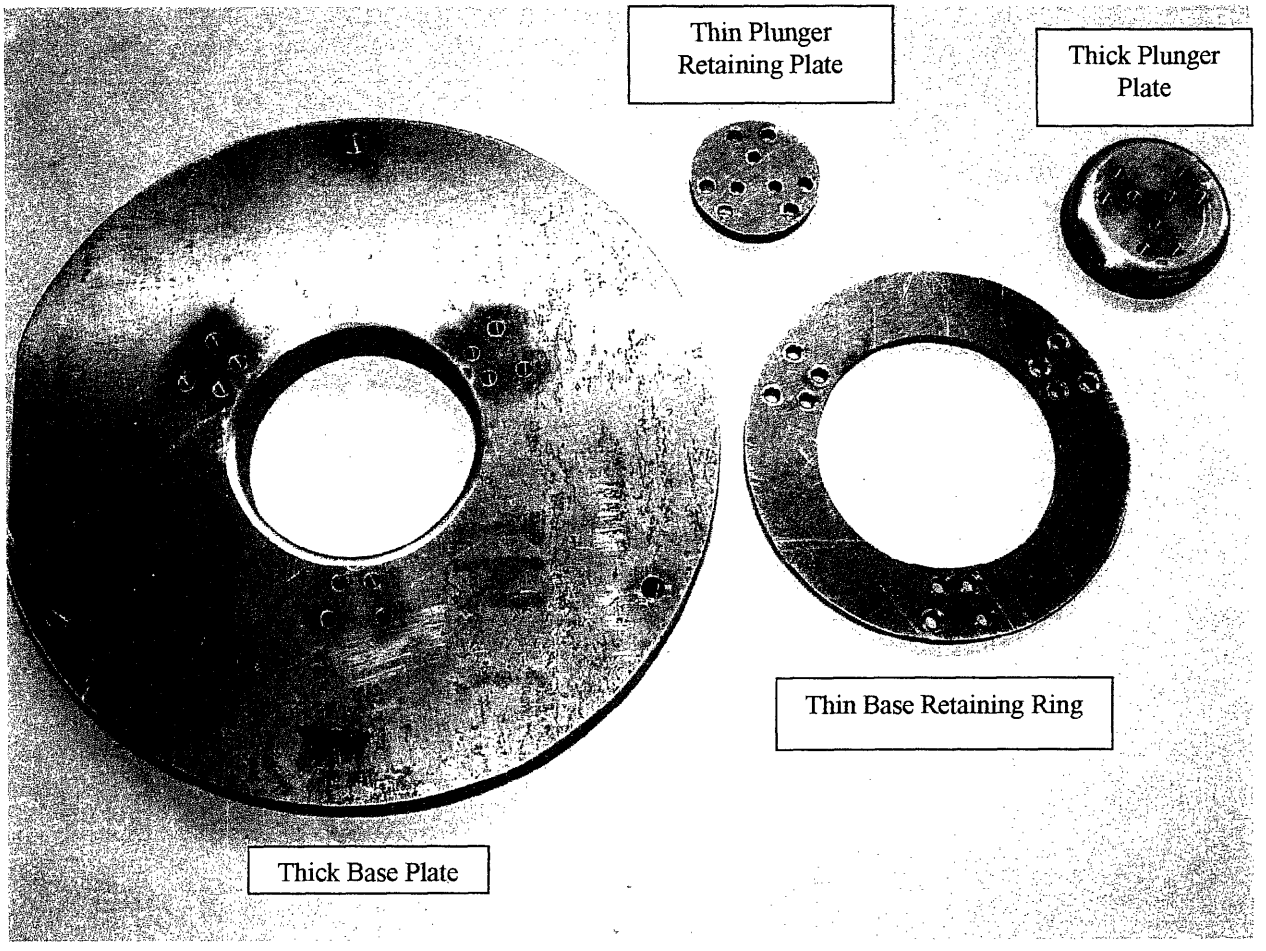

Figure 10: Tooling

The two large base pieces and the two small plunger pieces match, and in each case, the thinner part is bolted through the mechanism to the thicker part. In this way, two rigid units were created, separated by the thin members of the draw reserves, where the deformation was desired. During the actual forming process, the thicker parts were primarily responsible for providing the force bearing surfaces. That is, the thick plunger plate was pushed into the mechanism, which was resting on the thick base plate. The edges of these two thick parts were rounded off so the beam bending process was able to form around a larger radius of curvature than a sharp edge.

The tooling was cut out on the waterjet in varying thicknesses of metal, and then the holes in the thick pieces were tapped.

The method of positioning the mechanism on both the large base plate and the smaller plunger plate appears in Figure 11.

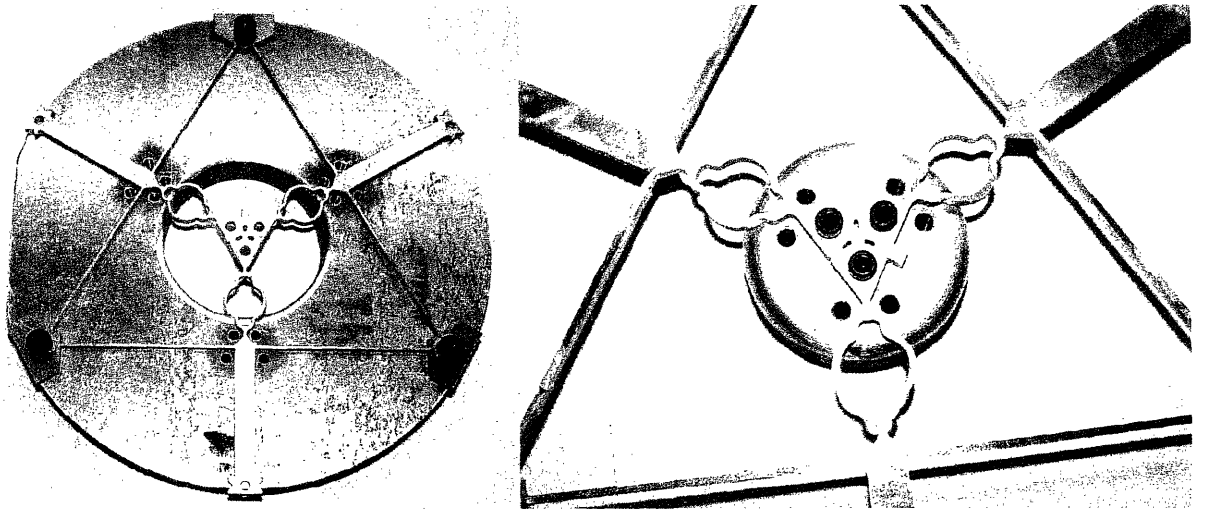

Figure 11: Positioning the 2D Mechanism on the Tooling

The positioning takes advantage of the location of known features. For the base plate, these are the same holes that are used for fixing the mechanism to the testing support. As seen in the left side of the figure, the puts the pivot region among four holes that will eventually receive bolts. The middle of the stage is now in the middle of the hole in the middle of the part. For the plunger plate, the three holes in the stage are used to locate the plunger with respect to the part. This brings their centers into alignment, and also puts each of the pivots between two bolt holes.

The cover plates and the retaining ring then are affixed through the bolt holes left open for them. For the plunger, because of the smaller size, the positioning bolts also pass through the retaining plate. By bolting the retaining plates down securely, the pivots are rigidly isolated from the exposed bending part. The actual forming takes place on an arbor press, as will be discussed in the Manufacturing section below. The fully assembled tooling with mechanism in place for processing is shown in Figure 12.

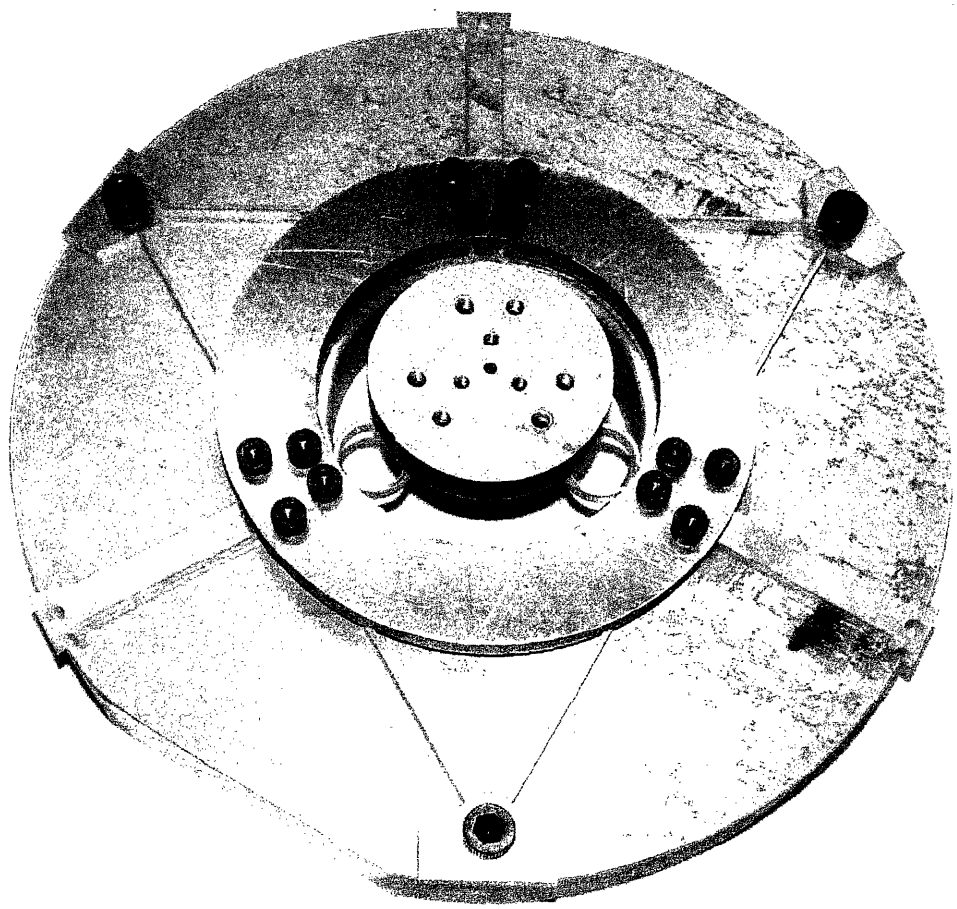

Figure 12: Fully Assembled Tooling and Mechanism, Ready to be Pressed

3.3 Testing Setup Design

The functional requirement of the testing setup was that it support the mechanism and bring the mechanism and actuators together to sufficiently allow for interaction between them. In addition, the setup was to allow room for the measuring devices to be positioned. Those functional requirements largely determined the design of the setup: the setup accommodated the mechanism as described above and standard micrometer heads in as little volume as possible to maintain proper rigidity. A picture of the resulting part appears in Figure 13.

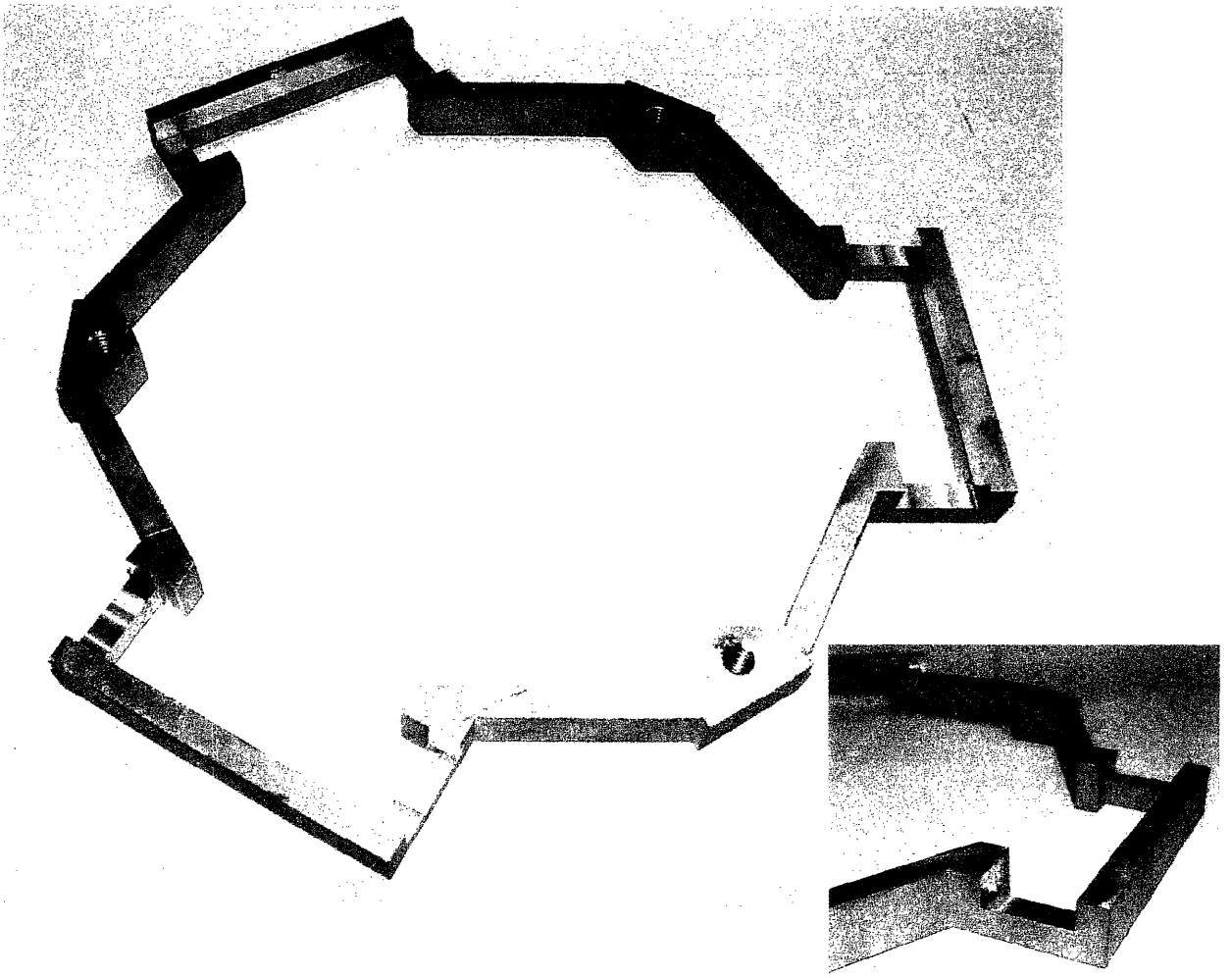

Figure 13: Testing Base, with Inset of Side Detail

The same pentagonal shapes are repeated from the mechanism, along with threaded holes to bolt the mechanism in position. These features support the mechanism relative to ground. This is important to take full advantage of all of the degrees of freedom during operation, as parts of the mechanism often deform below their initial unloaded position. In addition, when the rest of the parts are in motion, if any parts of the mechanism touch any other metal, it would result in rubbing and friction, which would translate to hysteresis of the output motions. The cutouts on the side are to accommodate the in-plane actuators: The neutral axis of the micrometer head actuators is designed to coincide with the middle plane of the lower part of the mechanism, itself

half of the thickness of the mechanism above the top plane of the test base. Thus, parts of the micrometer extend below the plane of the test base, and parts of the material must be removed to allow for clearance, as shown in the inset of Figure 13. This part was cut out on the waterjet, and then the cutouts were milled out and the holes tapped.

This structure has the additional advantage of being one continuous ring, so the attachment points for the mechanism are held apart at predetermined dimensions with good rigidity. The supports for the micrometer heads are shown in Figure 14.

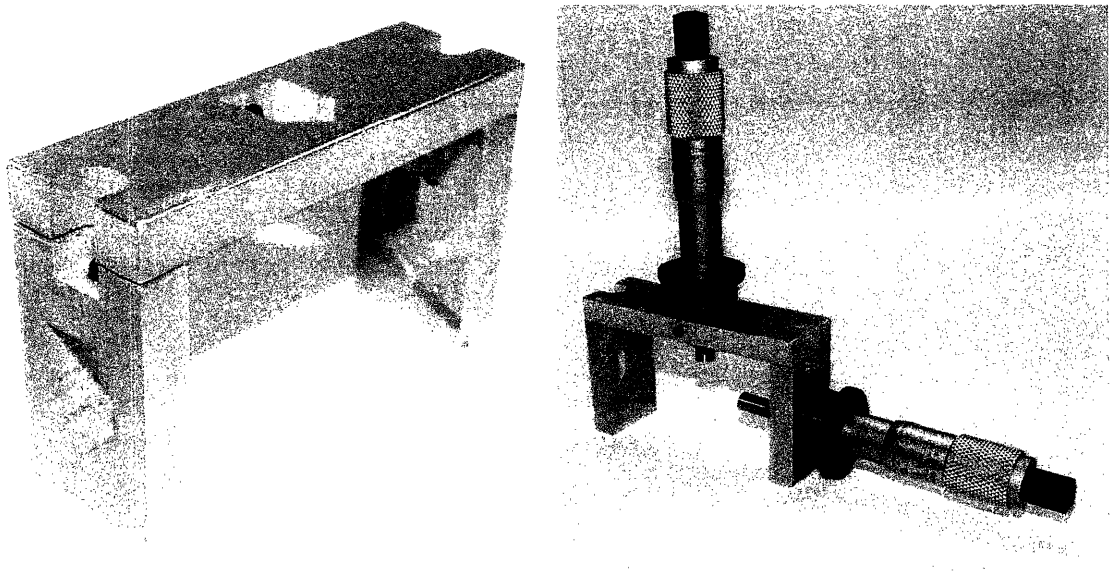

Figure 14: Micrometer Head Supports

These supports are designed to accommodate micrometer heads contributing input displacements in three directions: both directions in-plane, and one out-of-plane. The openings are tapered, so together with a set screw, there are three points of contact between the micrometer heads and the fixture. The parts were cut out on the waterjet, drilled and tapped for the set screws, and then attached with superglue. A picture of the mechanism tab, with ball bearings attached with superglue, on the test base, without the micrometer fixtures inserted, appears in Figure 15.

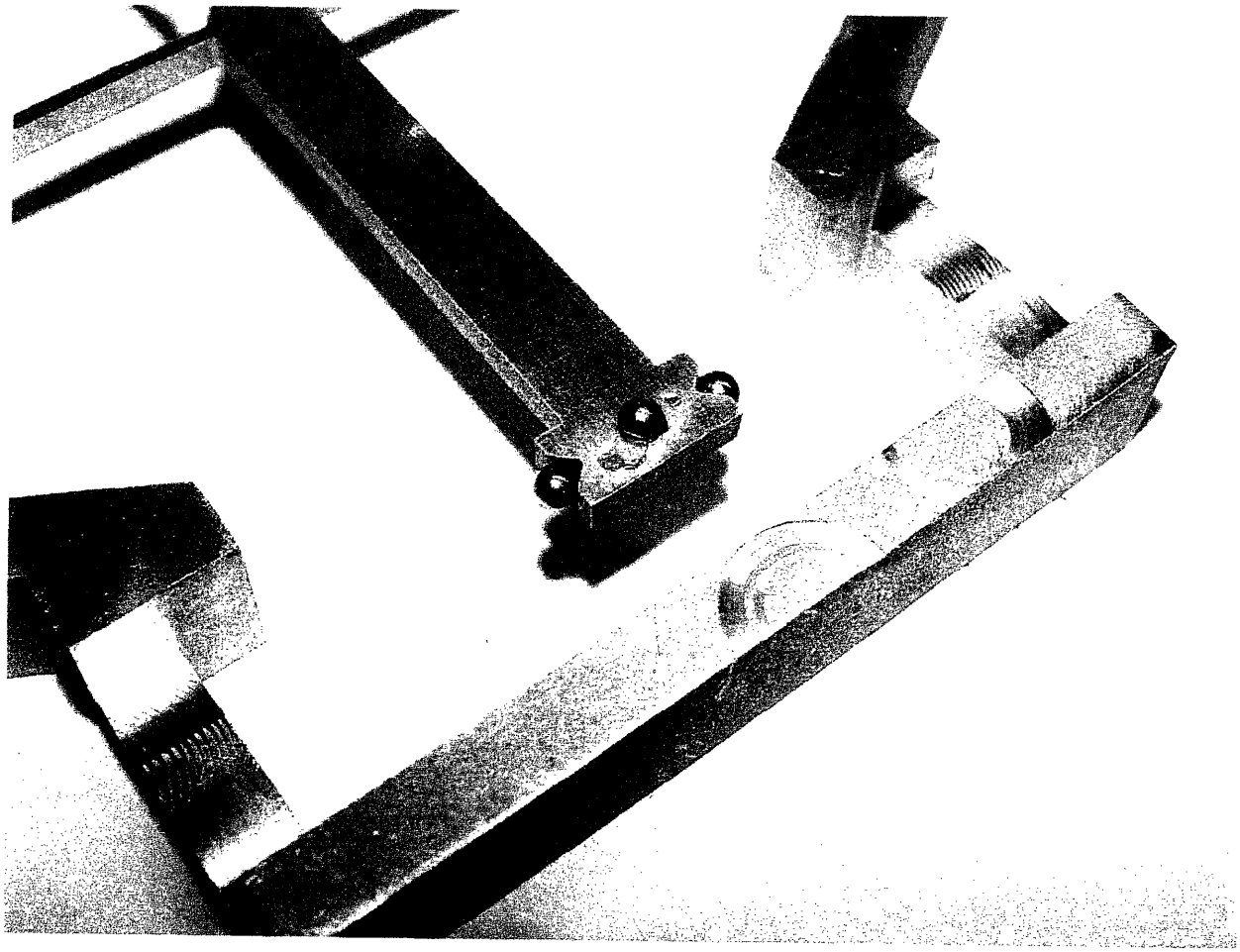

Figure 15: Mechanism Attached to Test Base, Micrometer Fixtures Not Attached

The circular rings seen on the top of the test base were where the end mill was touched off to determine the proper depth of cut for the channels. As the surface that bears the marks does not interact with the testing, this was acceptable.

The channels are centered on the plane defined by the three ball bearings, with enough room between the mechanism and the channel to fit the micrometer head and allow for sufficient range of motion of that actuator. A detailed picture of how the micrometer heads interact with the mechanism is shown in Figure 16.

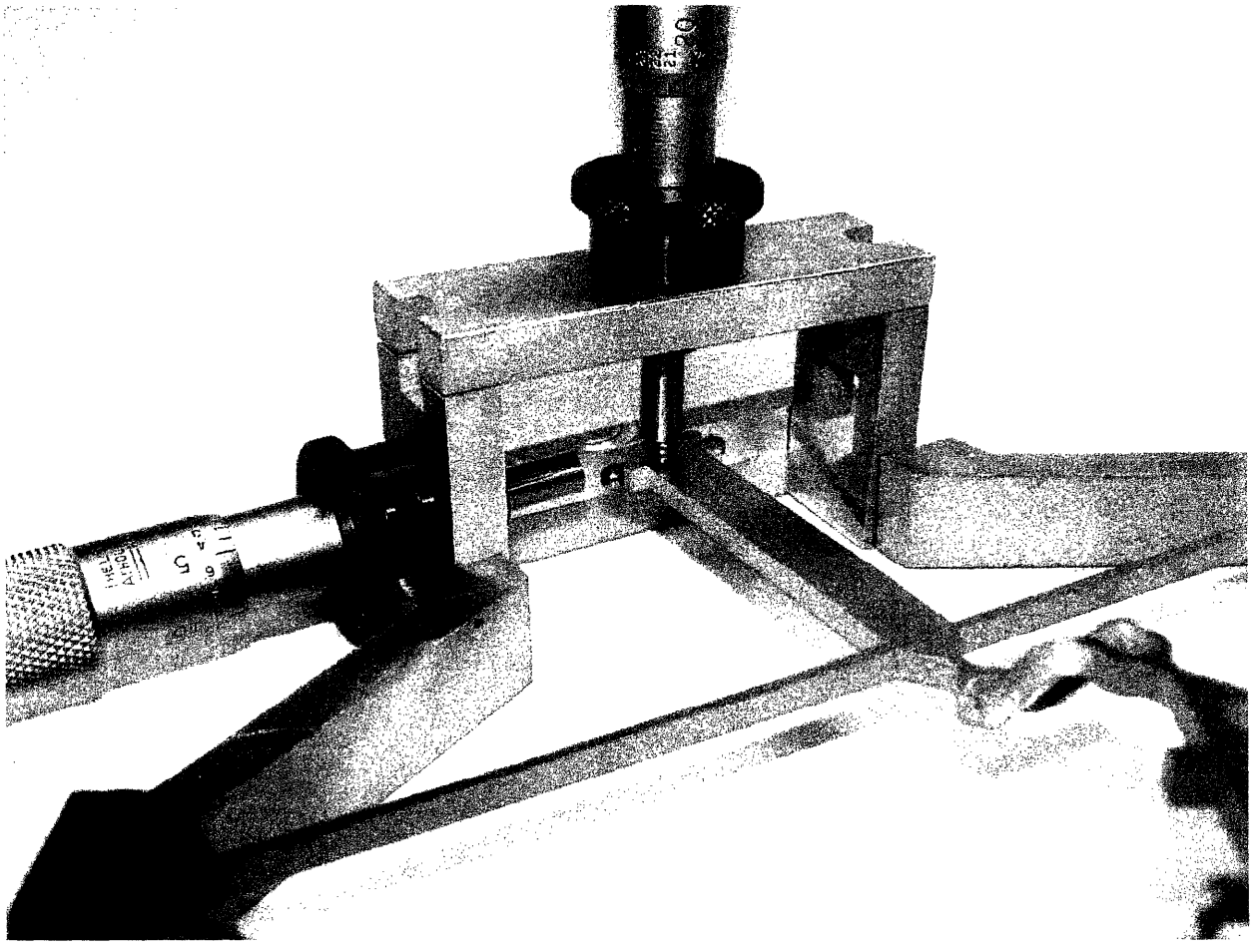

Figure 16: Micrometer Heads Interacting with Mechanism

While the width of the micrometer heads makes a simultaneous input of in-plane and out-of-plane displacement possible, this was never actually performed, and the figure merely portrays the possibility. The full test setup, with mechanism and micrometers, appears in Figure 17. It is clear that there is sufficient room to position a dial gauge. The exact positioning of the dial gauge, as well as the position of the capacitance probe, will be covered in the section on Testing.

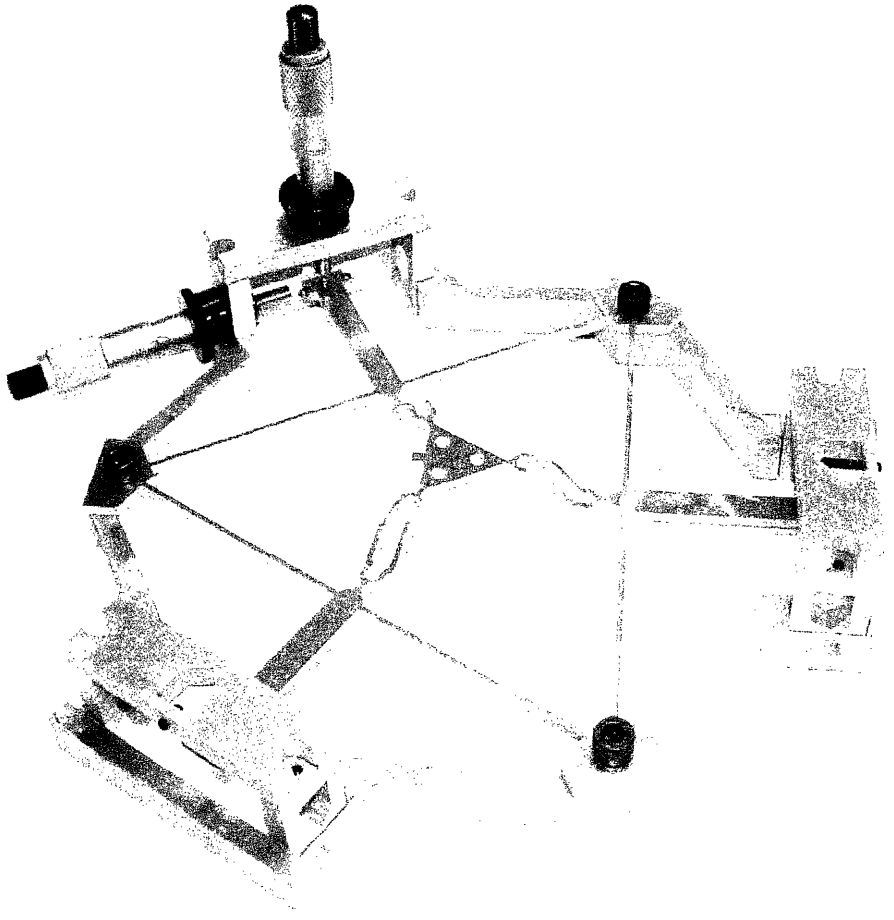

Figure 17: Test Setup, with Mechanism and Micrometers

3.4 Modeling and Analysis Design

In addition to the physical prototype, a model was created in SolidWorks that was evaluated with the assistance of the COSMOSWorks Finite-Element Analysis (FEA) Package. COSMOSWorks is designed to integrate directly into SolidWorks, though it only evaluates linear models. The creation of the model was relatively easy to do, as in order to cut the model out using the waterjet, a two-dimensional SolidWorks drawing had been generated. This was very easy to extrude, yielding the picture shown in Figure 18. This orientation is similar to that of the physical model portrayed in Figure 9.

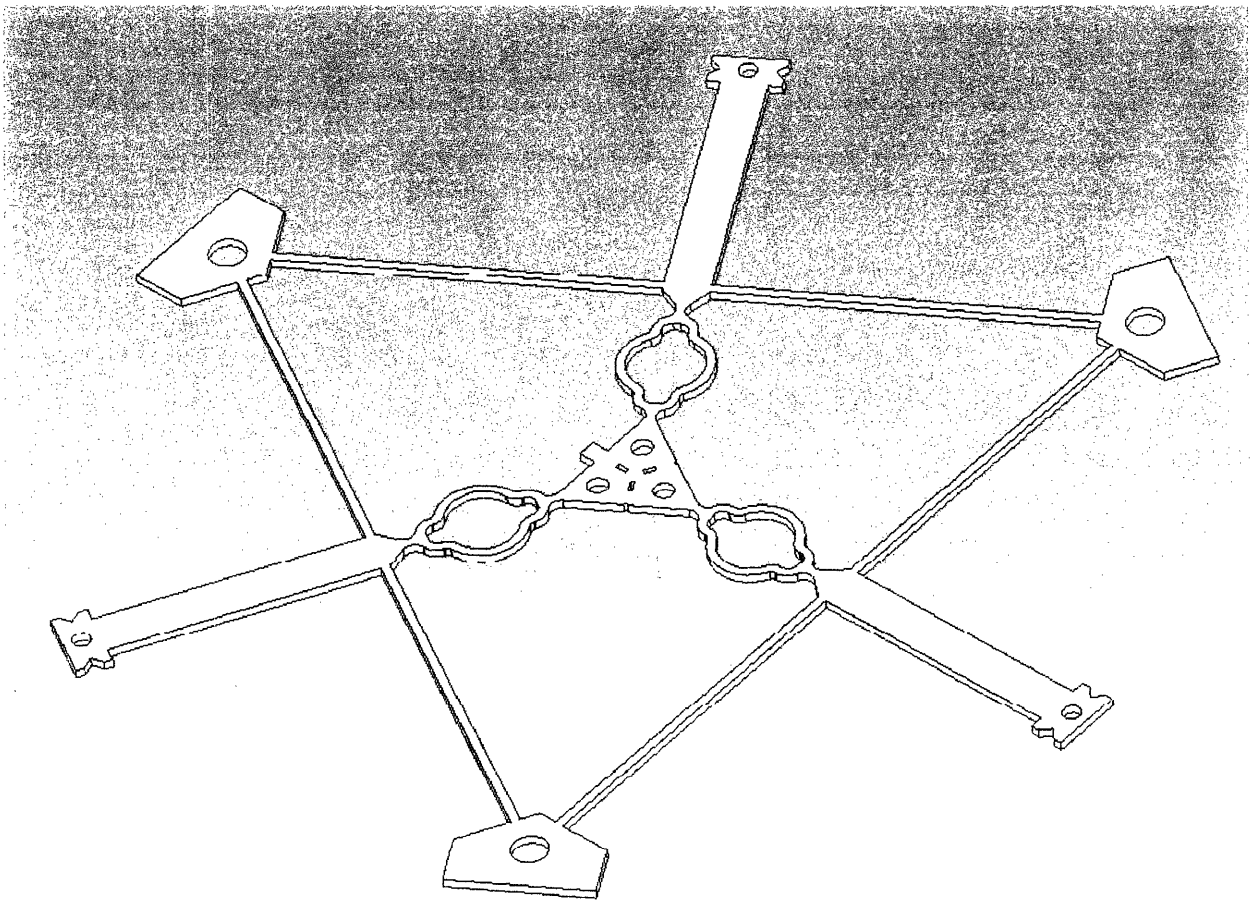

Figure 18: SolidWorks Model of 2D Part

While it was not possible to virtually plastically deform the model into the final three-dimensional virtual mechanism, using this FEA package, it was possible to create a realistic facsimile of the three-dimensional model. This model appears in Figure 19.

It is important to remember that this computer model is fundamentally different from the physical model. SolidWorks and COSMOSWorks will treat it as a normal, isentropic part that has never been deformed. In reality, due to the plastic deformation, there are mechanical and material effects, such as residual stress concentrations, strain hardening, and rearrangement of

the grain boundaries, to name a few. However, for a first-level approximation, this model is sufficient.

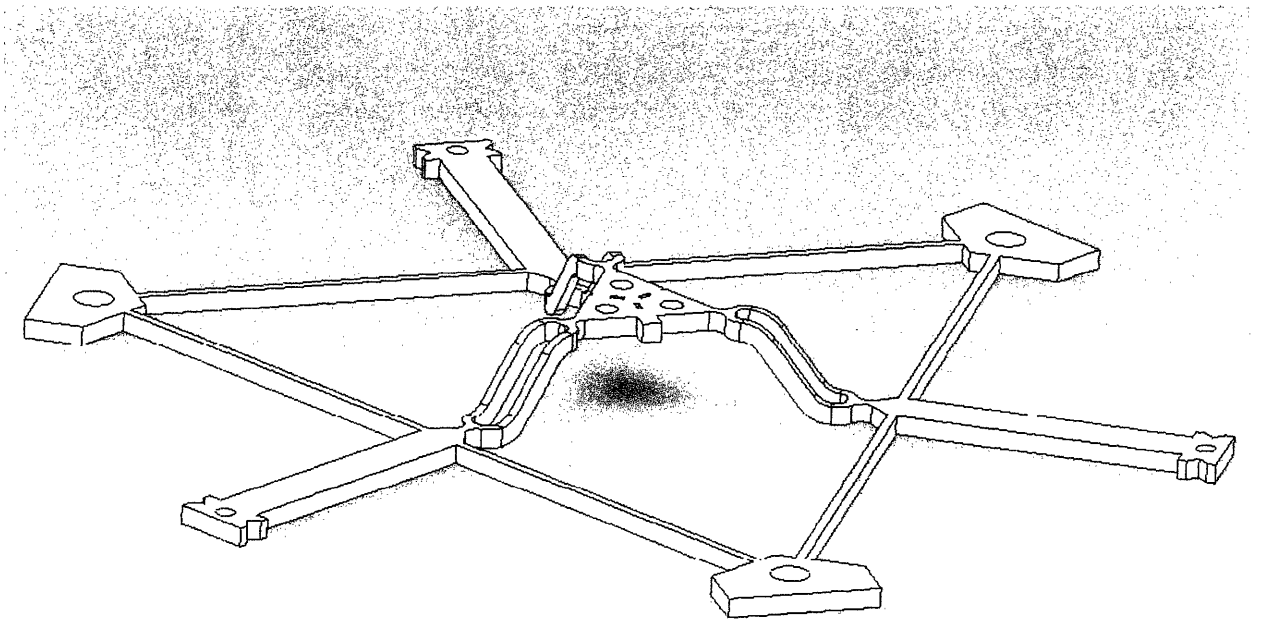

Figure 19: SolidWorks Model of 3D Mechanism

The solid model and the FEA will predict an input relationship for the tests to be performed in Section 5. FEA is necessary as the geometry defies a simple analytical solution. The Finite-Element Analysis will also reveal the loading conditions that will cause the mechanism to reach yield stresses, which, as discussed above, in the operating regime, will be avoided.

4.0 Prototype Manufacturing

The steps in creating the prototype have largely been discussed above, but a pictorial review of the process appears in Figure 20.

4.1 The Manufacturing Process

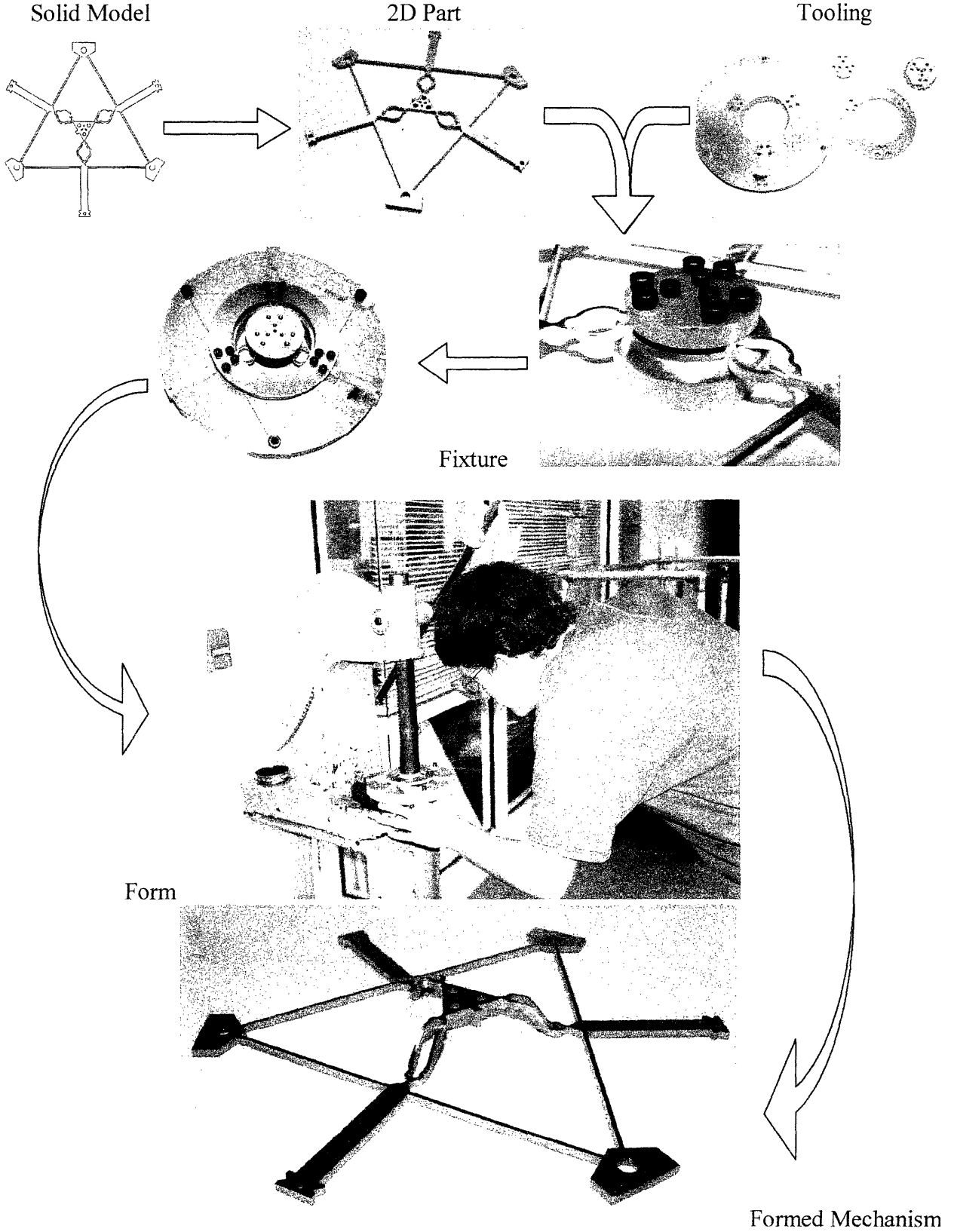

Figure 20: Steps in Creating Mechanism

The part is first cut out on the waterjet. Then, after filing to remove burs, it is bolted to the tooling. The full tooling and mechanism is put in the arbor press, where it is pressed to form the three-dimensional part.

As can be seen from the diagram, the arbor press is not a precision instrument. The amount of deflection of the mandrel was controlled by the experimenter "eyeballing" the draw reserves until they appear to be approximately straight. It almost does not need saying, but this process was neither repeatable nor accurate, and any future work would seek to find a better way of controlling the forming process. However, even with this drawback, the resulting mechanism was conformed well to the design. A close-up of the deformed legs appears in Figure 21.

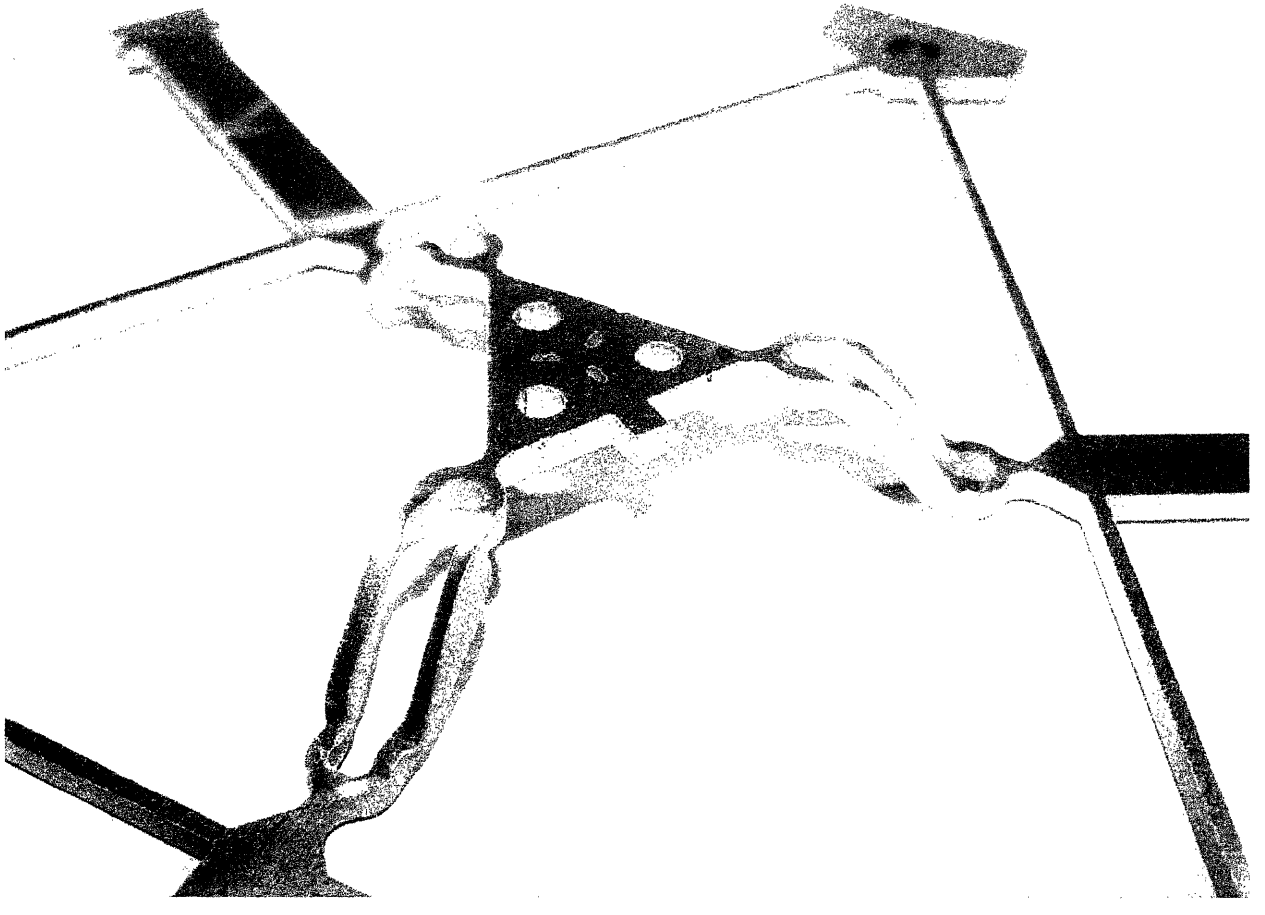

Figure 21: Deformed Legs and Stage

It is important to note the fact that, as desired and designed for, the compliant pivots are untouched by the process. However, the prototype does not conform geometrically to the ideal computer model portrayed in Figure 19. It appears that as a result of the friction between the tooling and the legs, as the legs straightened, they twisted. The twisting, as well as the stresses inherent to the bending process, seems to also have caused some slight necking and earring at the corners of the legs.

These two phenomenon are the potentially unpredictable effects discussed above. It will be up to the testing to evaluate if these are having a significant effect that detracts from the performance of the mechanism or not.

4.2 Failure Modes Encountered in Fabrication

In the forming of the multiple mechanisms, a few parts failed. Failure always occurred during the pressing, as that is the only time during the two-step fabrication when sufficient force is applied to fail the mechanism. Figures 22 and 23 show two primary modes of failure.

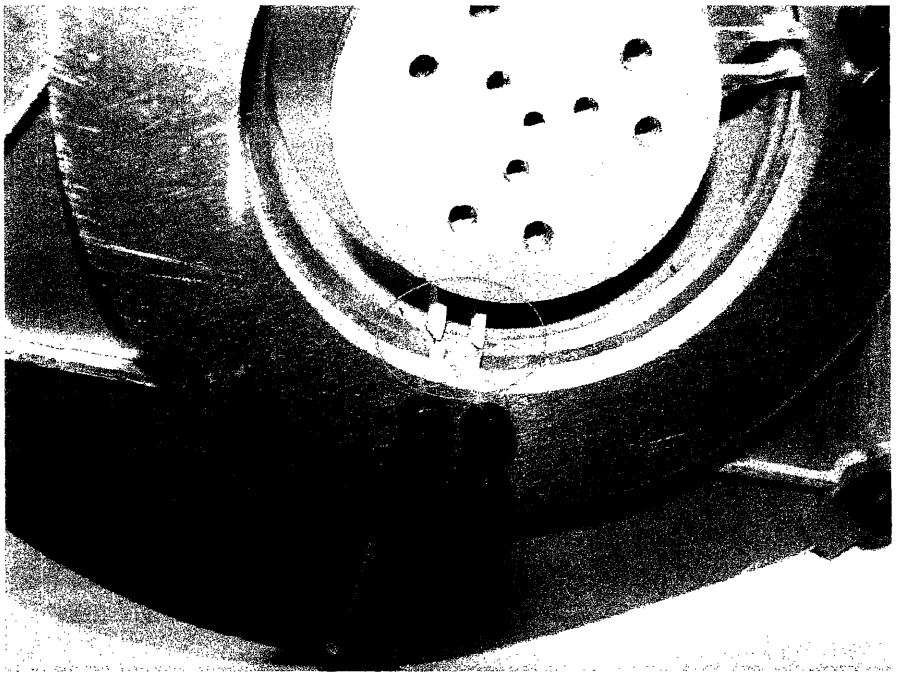

Figure 22: Failure Due to Over-Pressing

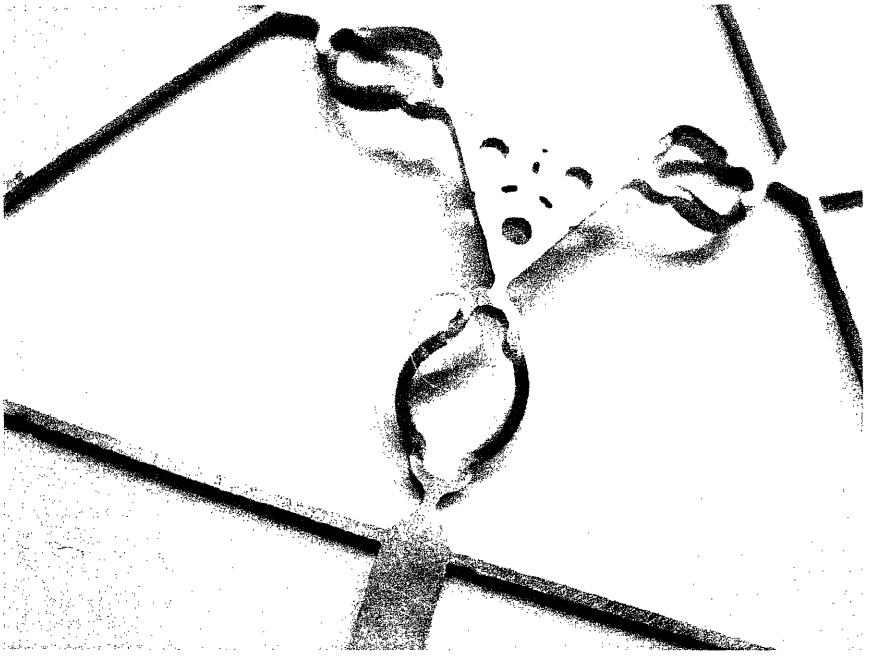

Figure 23: Failure Due to Excessive Stress Concentration

The first failure occurred because of manual pressing: the mandrel was pushed too far, and the legs were no longer undergoing beam bending, but instead simple tension loading. The aluminum necked and the legs failed at the point where the radius of curvature was smallest.

The second failure also occurred during the pressing process, but far short of the completion of the plastic deformation process. This can be seen in the shape of the legs; they remain bowed, although there has clearly been some deformation, as the stage is above the plane of the tabs. Examination of the part revealed dimples caused by the waterjet process on the bottom surface. These dimples are created if the jet of water is diverted from a perfectly vertical stream, as occurs in the leading in and leading out from the primary cut. By reducing the cross-sectional area at this point, the stress concentration rises, leading to premature failure.

The fabrication process is not yet perfect, but it was able to succeed in creating viable working parts, which were tested, as reported in the next section.

5.0 Testing

To determine if the mechanism was behaving according to the model, a number of tests were performed.

5.1 Displacement Response Test

This test consisted of pushing the ends of the tabs some amount in given configuration and recording the resulting movement of the stage. Three such tests were run, with the input/output conditions portrayed in Figure 24.

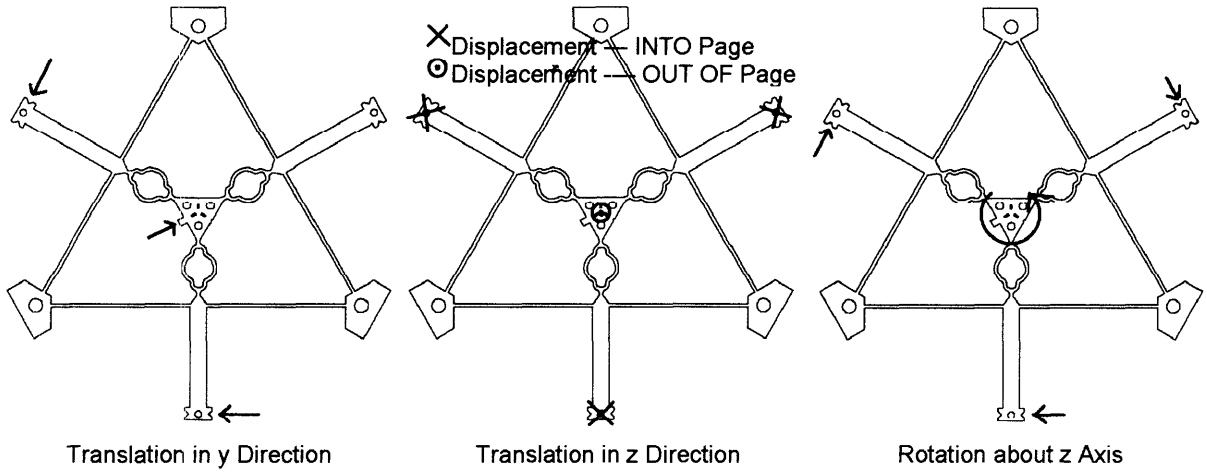

Figure 24: Configurations of the Three Displacement Response Tests

The advantage of these three configurations is that they all involve identical magnitude of displacements at the two or three inputs, so it is easy to scale the test as a function of one variable, the magnitude of displacement of each input point.

The input was achieved by the micrometer heads, which create displacement inputs by their very nature. The output was measured using the dial gauge. An example of the positioning of the dial gauge appears in Figure 25. In this figure the micrometer heads are still in the example configuration of Figure 16, but the dial gauge is in the actual position where it measured displacement in the z direction. The dial gauge was glued to blocks of appropriate size to achieve the desired orientation and position for each test. For the rotation about the z axis test, a cantilever arm was glued onto the central stage that amplified the motion and extended it out past the end of the test setup. By measuring the radius of the point of measurement from the center of the stage, the angular measure could be extrapolated.

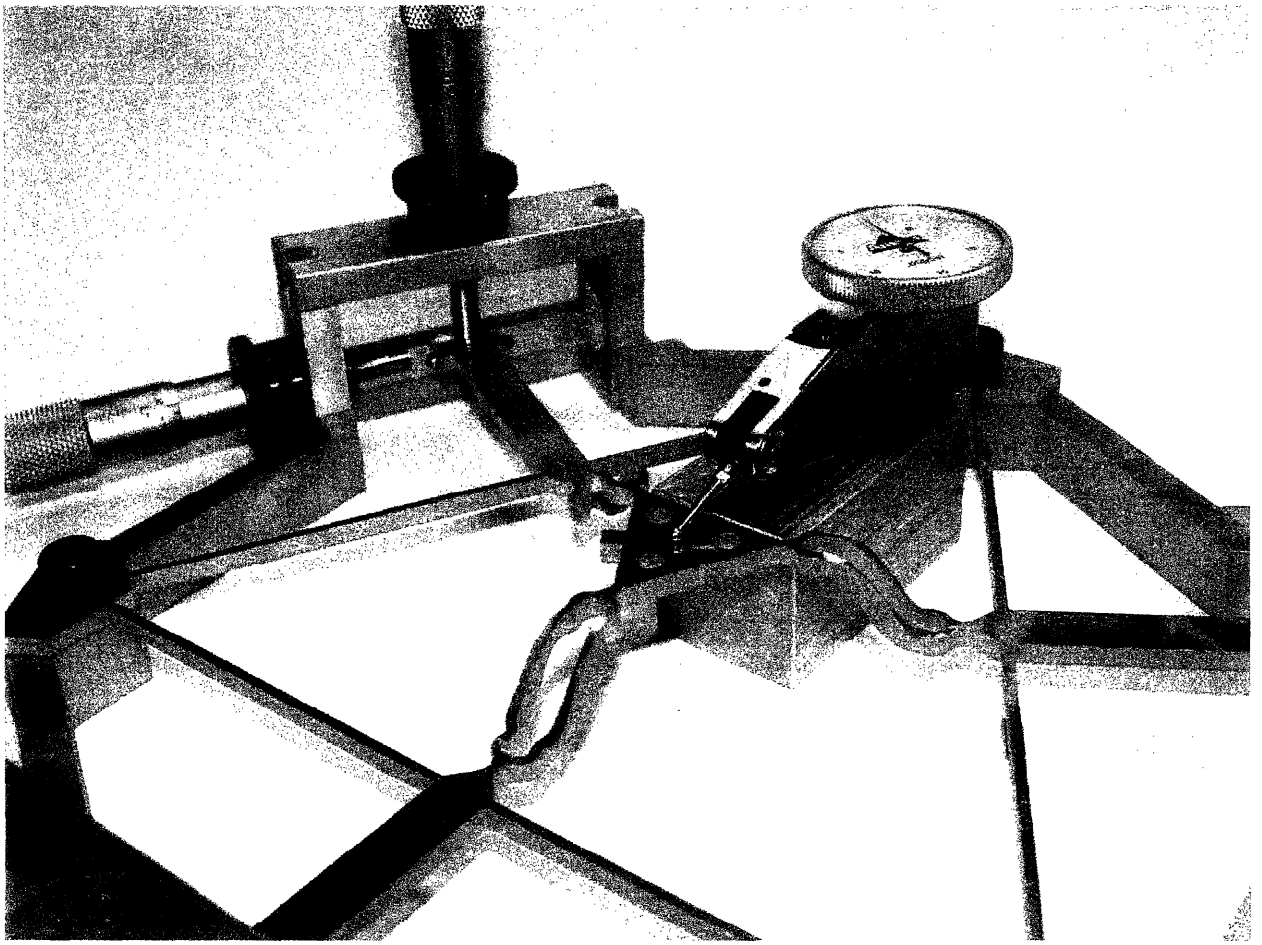

Figure 25: Position of the Dial Gauge to Measure Displacement in z Direction

To obtain the ideal range of input motion that would stay below the elastic limits, as well as the predicted output motion for comparison with the experimental data with, the FEA model was employed. Full details of the derivation of the expected data appear in the Appendix, and Figures 26, 27, and 28 show the results in graphical form.

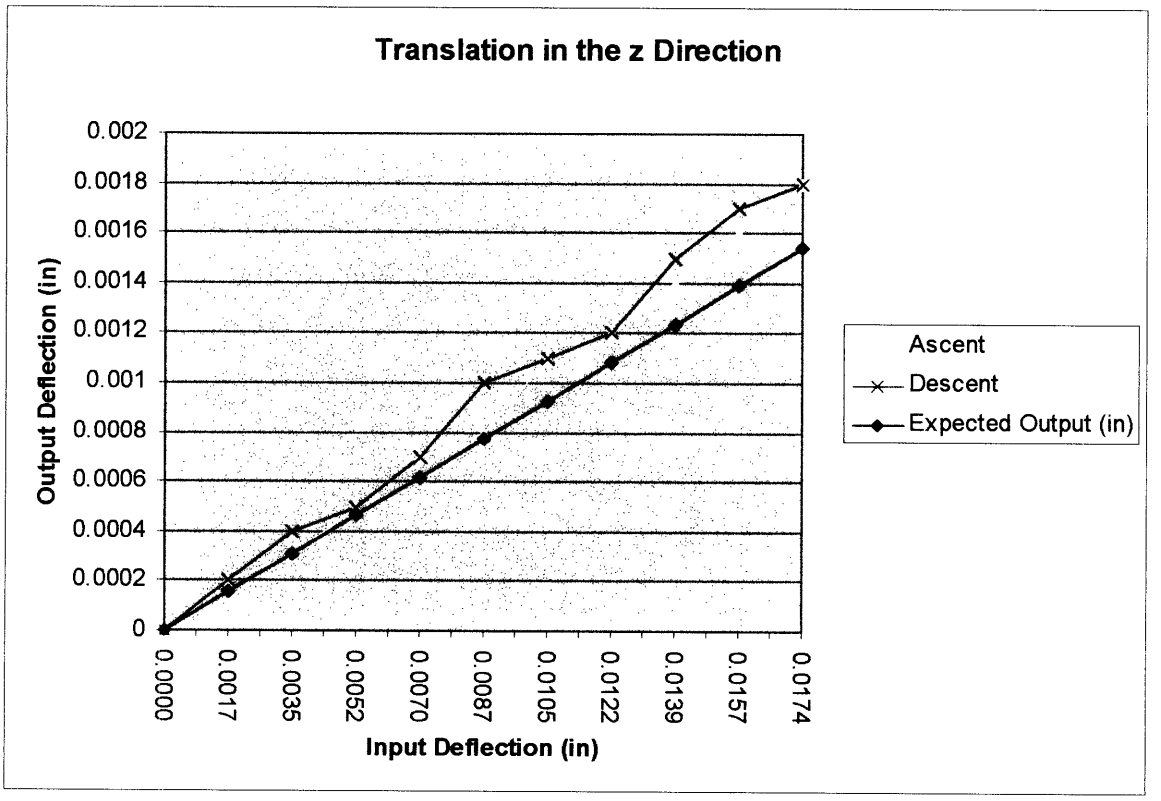

Figure 26: Results from z Translation Test

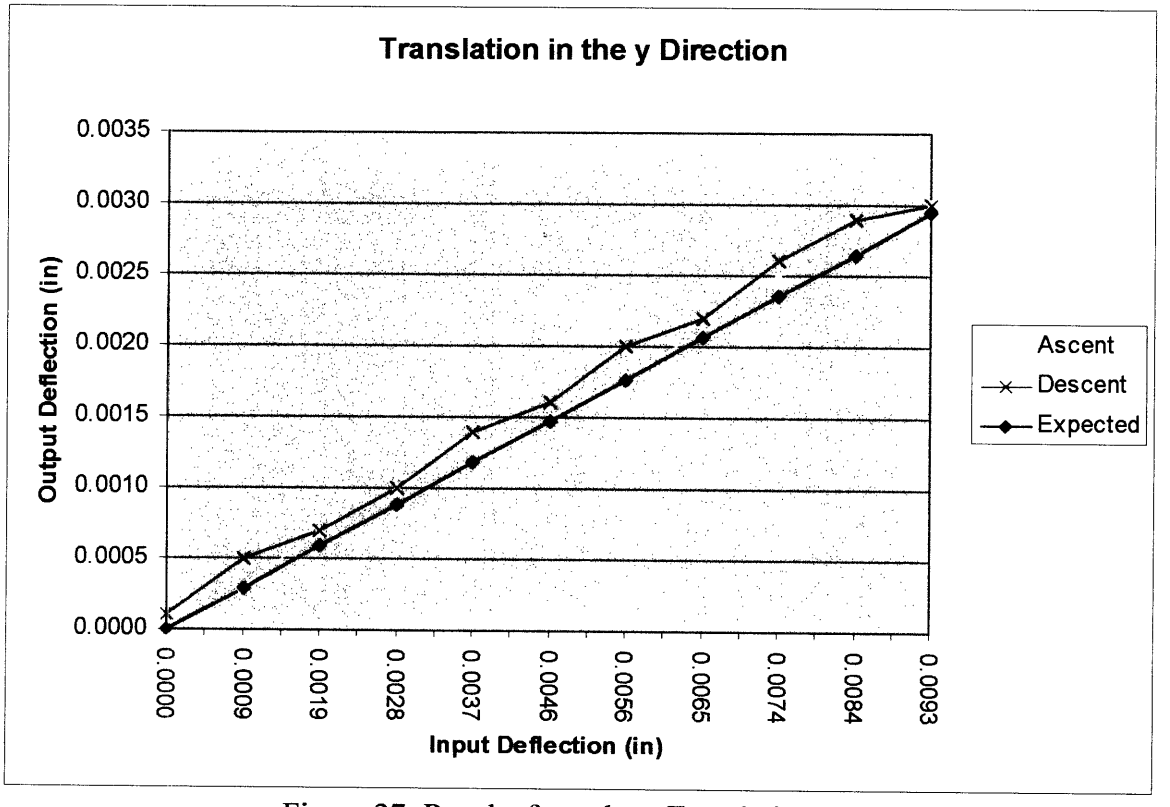

Figure 27: Results from the y Translation Test

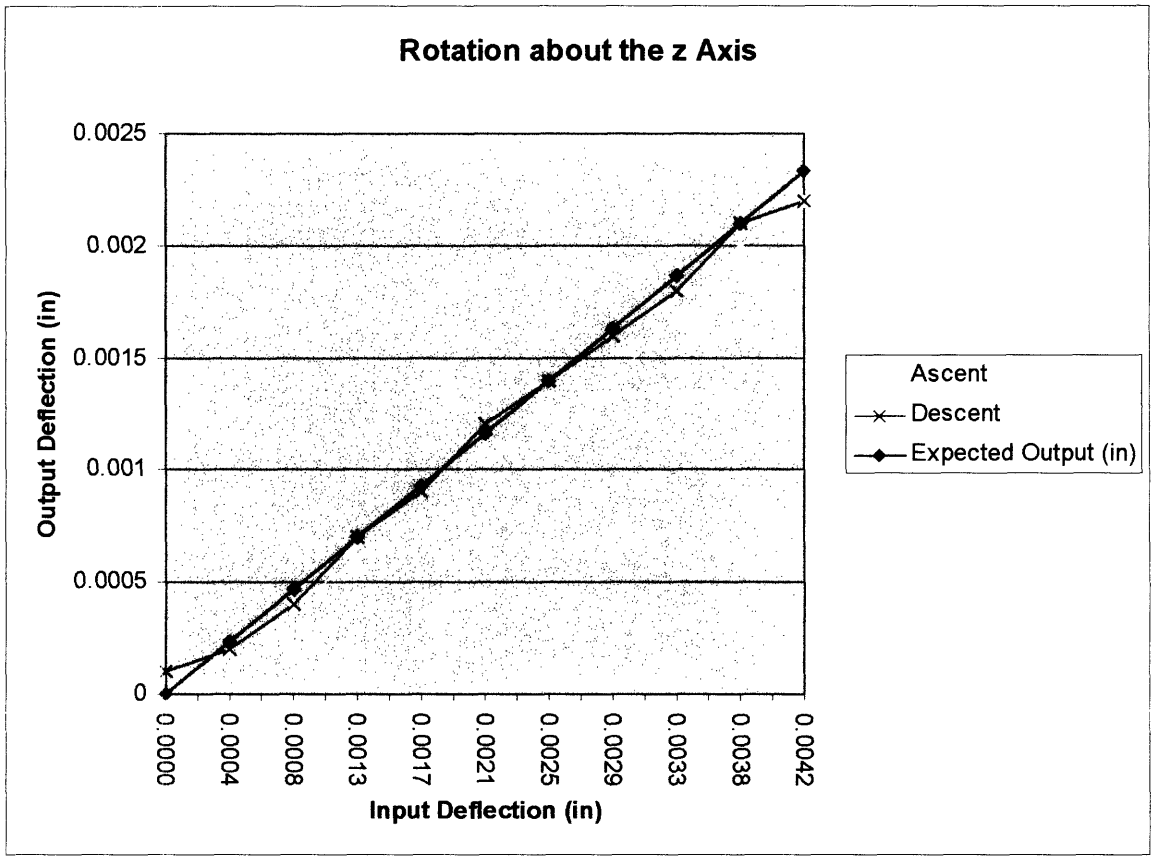

Figure 28: Results from the θ_z Rotation Test

Each of these graphs has three sets of data. The set that forms the straight line is the expected output. The other two are an "Ascent" data set and a "Descent" data set. The former was the data gathered as the input displacement was increased, and the latter was data gathered as the input displacement was decreased back to zero. Tracing the points chronologically, one starts at the (0,0) value of the ascent graph, goes up to the maximum value, and then follows the descent graph back down. It is for this reason that the ascent and descent share the data point at the extreme value of input deflection on each graph; it is because it is the same value.

This ascent/descent data was gathered to investigate the potential effects of hysteresis. As can be seen, there are small deviations in the two paths, possibly caused by limitations in accuracy of the experimental processes of micrometer head actuation and dial gauge sensing. It is also possible that friction between the balls and micrometer heads is at work, though the

largely erratic behavior of the error does not provide a good picture of one trend. However, whenever there is a misfit between the ascent and descent data sets, it is with the descent having a higher value, which does point to some amount of hysteresis. It is also possible that the hysteresis is at work within the micrometer head actuators themselves, as they are known to exhibit self-hysteresis.

5.2 Stress Relief in the 24 Hours after Processing

The next test performed looked at the effects of stress relief in the short-term after the plastic deformation, to see if visco-elastic effects were affecting the performance of the mechanism. To perform this test, a sample part was plastically deformed in the machine shop with the arbor press and then conveyed immediately to the lab (roughly 15 minutes transport time), where it was affixed to the test setup and measured for the next 24 hours.

As the mechanism is three-way, in-plane symmetric about the center of the stage, the most noticeable effects, were expected to be seen in the z direction. Thus it was most important to measure in the z direction. Future work will seek to measure the response in the other degrees-of-freedom. The expected position drift would be on a micrometer-level scale, and data would be gathered over the course of an entire day. As a result, it was decided to measure the displacement with a capacitance probe and record the data automatically with the computer.

To do this, a program was written in Simulink, a development environment in MATLAB specifically geared to system control and signal processing. This program was then uploaded into ControlDesk, a program designed to interface with dSPACE, an Analog to Digital converter attached to the computer. The capacitance probe was fed through an amplifier to dSPACE, and from there the data went to the computer, where it was logged for 24 hours. Figure 29 shows the

test setup for this test, before the mechanism was attached. The capacitance probe is the cylinder sticking up through the block of metal in the middle, with the wire coming out the bottom. The block of metal is merely a pre-existing fixture that was drafted into service rather than requiring fabrication of a completely new fixture to do the same job. As the capacitance probe is about two inches long, it was necessary to increase the height of the test base used earlier, and that is the function of the stacks of block. Carbon-impregnated superglue was used to hold it all in place, and that is the black substance seen in the picture.

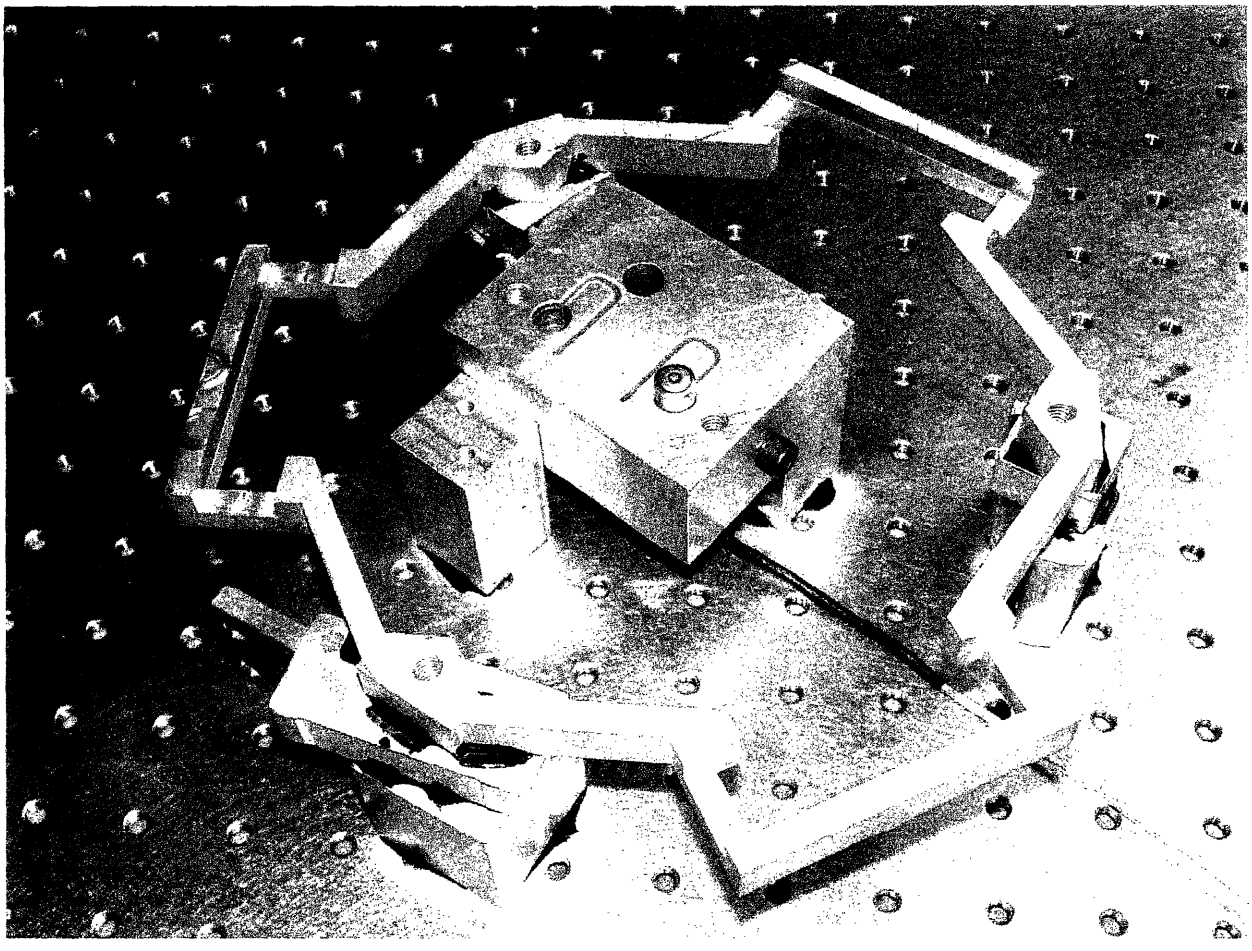

Figure 29: Test Setup for Post-Processing Position Drift Experiment

Once this was in place, it was necessary to modify slightly the test mechanism to interface correctly with the capacitance probe. For the capacitance probe to take accurate

measurements, it must be facing a smooth area of metal. The capacitance probe, as might be guessed from the name, measure displacement not by contact but by the changing capacitance between the probe and the target as the distance between them changes. As is, the stage has a number of holes, which could make it unsuitable. Figure 30 shows the solution: a block of the right size is attached to the underside of the stage to act as the target. The small slit in the block was used to insert the grounding wire for the capacitance probe.

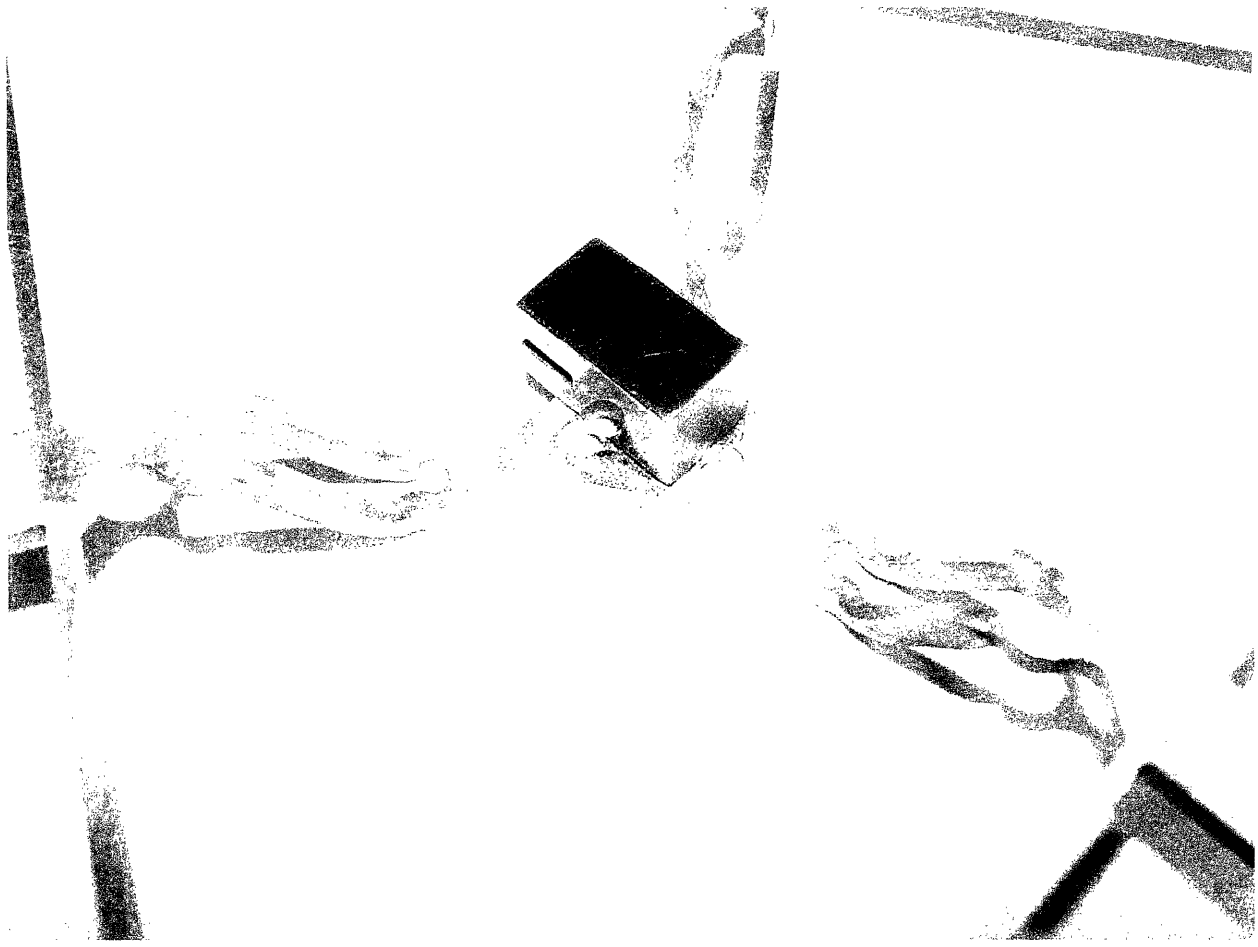

Figure 30: Block Attached to Underside of Stage to Act as Capacitance Probe Target

Putting it all together, the complete assembly, with mechanism installed and target block glued in place, appears in Figure 31. The inset is a closer shot of the interface between the

capacitance probe and the target. As can be seen, the sensing block is very close to the probe, but it does not touch.

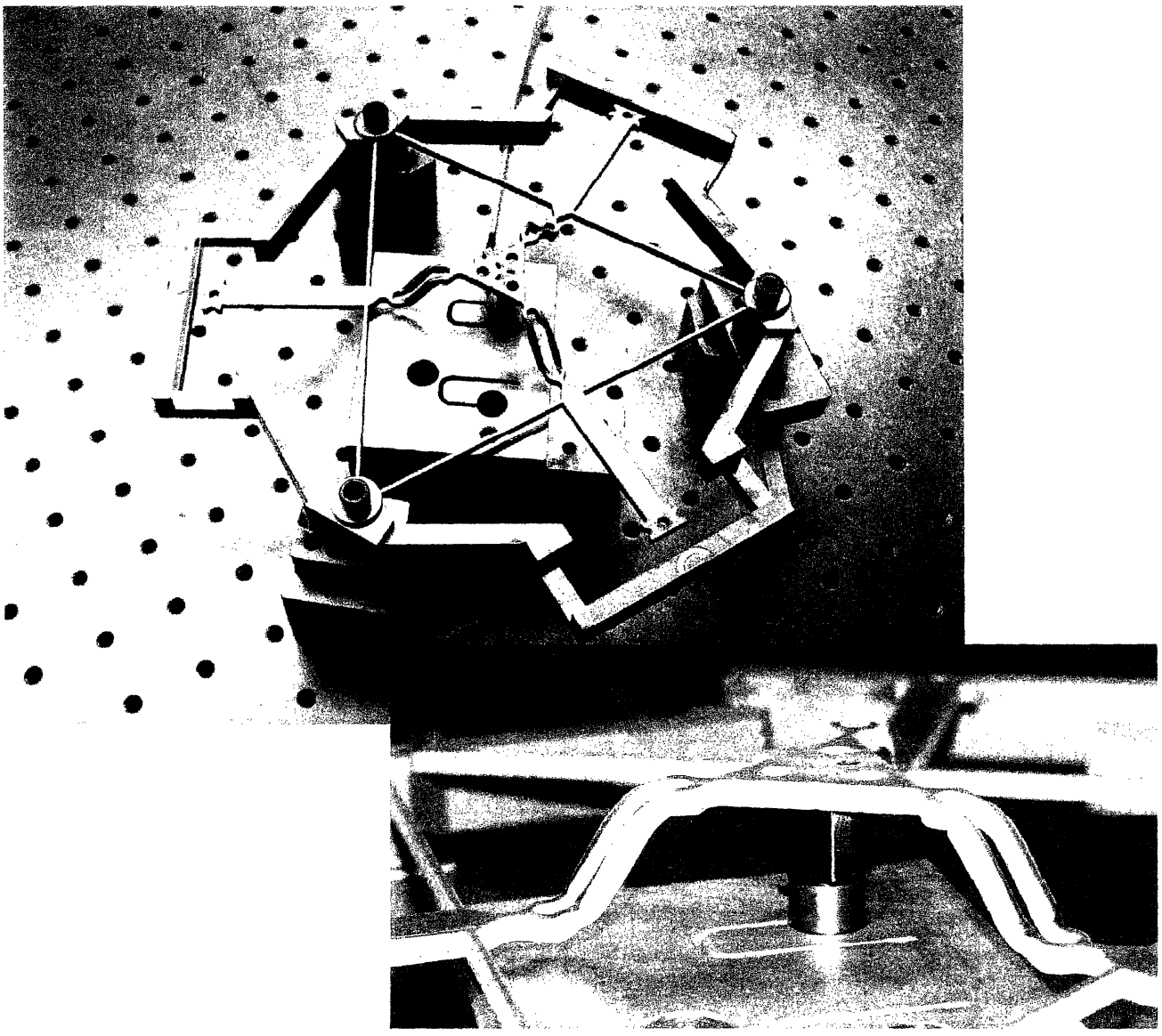

Figure 31: Complete Test Setup for Post-Processing Position Drift Experiment

From there, the test setup was covered with a large foam box to minimize the effects due to thermal expansion and contraction of the mechanism. The complete setup on the floating optical table, with the mechanism placed within the pink box and the amplifier for the capacitance probes sitting in the foreground, appears in Figure 32. The table was floated, using

the compressed air in the yellow cylinder visible in the corner of the Figure, to minimize the effects of the vibration of the room or building on the results. Even with this emphasis on decoupling the experiment from its surroundings, thermal expansion and contraction over the course of the day still played a large role in the data.

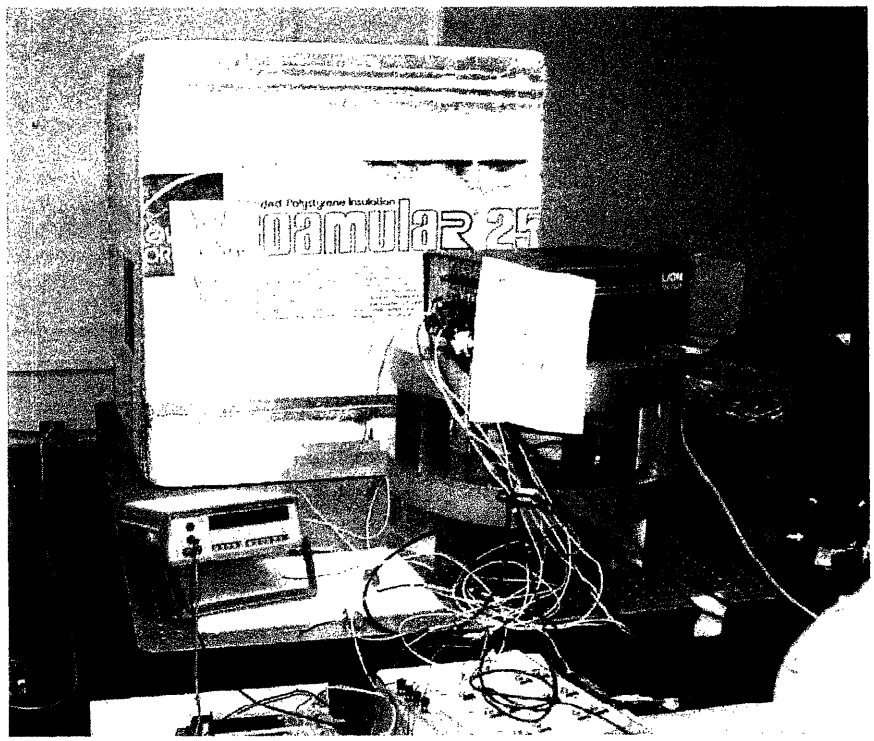

Figure 32: Post-Processing Position Drift Experiment

It should be noted that between travel time from the shop to the lab, setup time for the experiment and the computer program, time spent affixing the target block, arranging the setup, and activating the table, there was a gap of almost one hour from fabrication to commencement of test. Thus, while the test begins at t = 0, it is more accurate to think of it beginning at t = 1 hour post-processing. Two assumptions are reasonable in this case. The first is that if a clear trend is observed over the course of the 24 hour test, such as an exponential curve, it could be extrapolated backwards in time to right after the forming of the specimen. The second is that this may not even be an issue that effects the operation of the mechanism, because any

implementation wherein the mechanism would be formed and then immediately thereafter inserted into an operational setup would have at least a similar gap.

In addition to the short-term test, the same specimen was tested a week later in nearly identical conditions: test initiated at the same time of day, in the same location, using the same capacitance probe. The primary factor that had been altered between the two tests was that the specimen was no longer in the short-term post-processing regime. The visco-elastic effects had presumably subsided, so it was a good way to compare the relative effects of the thermal expansion and contraction. The results of these two tests appear in Figures 33 and 34.

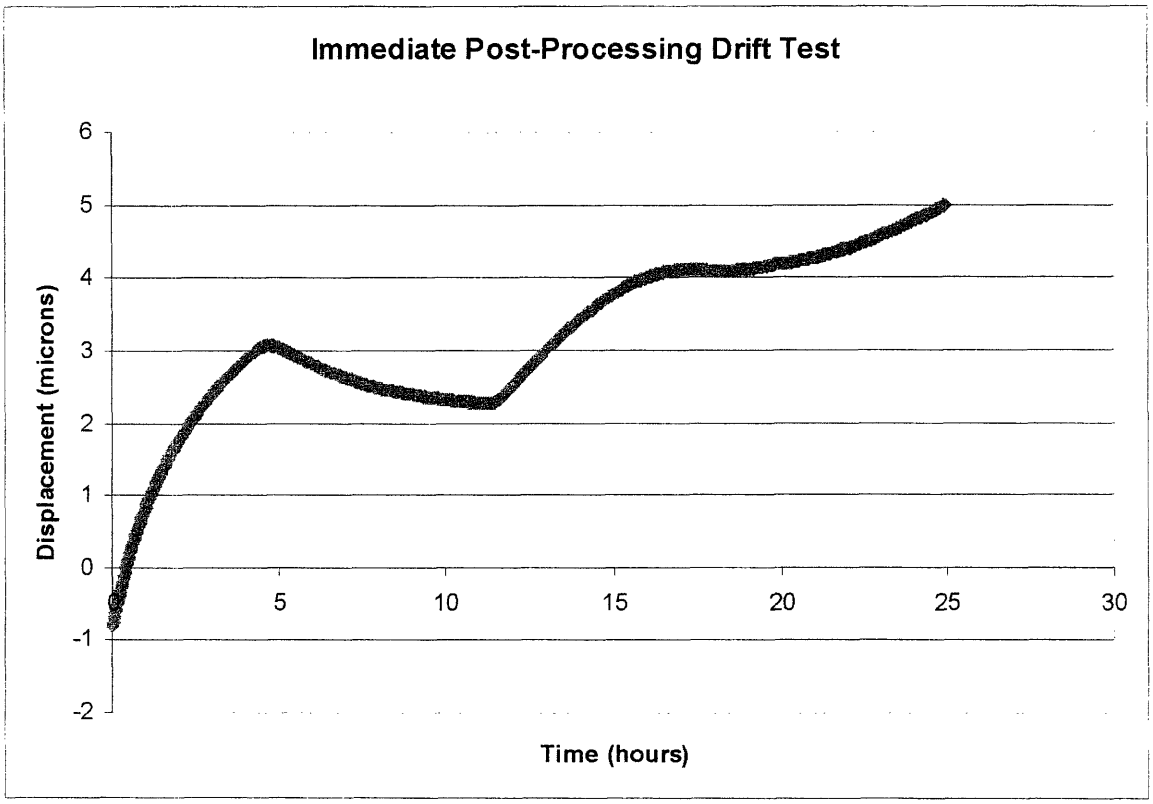

Figure 33: Results of the Post-Processing Position Drift Test

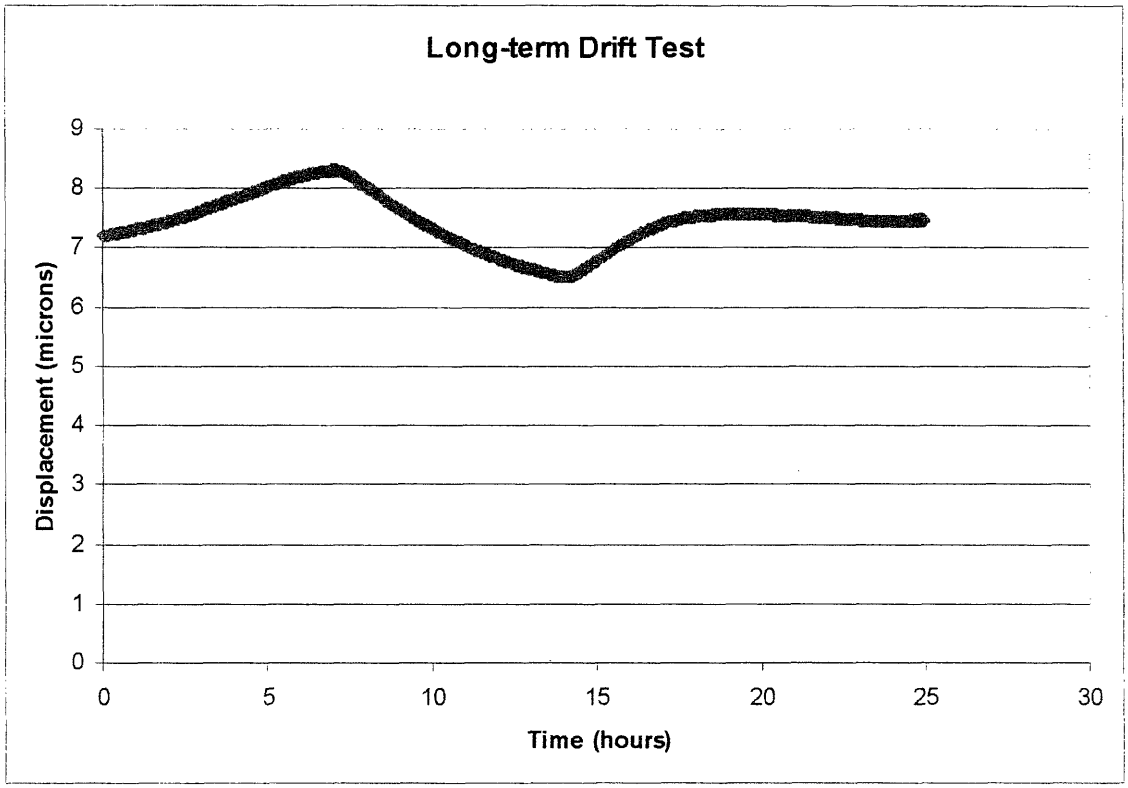

Figure 34: Results of the Longer-Term Position Drift Test

The capacitance probes are useful primarily for measuring relative movement over the course of one experiment; thus, for Figure 33, it is more important that the measurement grew six microns over the course of the test than what value it actually began and ended at, as those were determined by the experimenter setting up the equipment, not by any sort of calibration. Also, the graphs are inverted relative to the reference frame; an increase in the displacement value portrayed on the graph corresponds to a decrease in the gap size between the capacitance probe and the target – a lowering of the stage.

What is seen is a noticeable position drift over the 24 hour period in the short term test. During the longer-term test, the fluctuations are completely due to thermal effects. The fact that the test begins and ends at approximately the same value supports this theory, because the temperature varies in a 24 hours cycle in the laboratory.

In fact, if one can imagine subtracting from the short-term graph the deviations of the long-term graph from that graph's mean, a more striking exponential curve is evident with a time constant on the order of hours. At the end of the twenty-four hour test, it does not seem like the mechanism has finished contracting, but it is clear that by a week later, contraction is complete.

5.3 Creep Test

A final test was performed to investigate the effects of creep on the performance of the Nanomanipulator. Here too, the FEA was used to help decide the proper loading for the mechanism, as all creep effects are contingent upon the existence of prolonged stress in the part.

Since the test mechanism was set up to measure in the z direction, and prolonged loading in the z direction is easily achieved by hanging a weight from the end of each tab, creep in the z direction was evaluated. The FEA predicted yield stress would be achieved for a loading of 3 Newtons out-of-plane at each of the tabs. Thus, 300 g were hung from each of the tabs, and the same program was run for a day to measure displacement in the z direction. Results are in Figure 35.

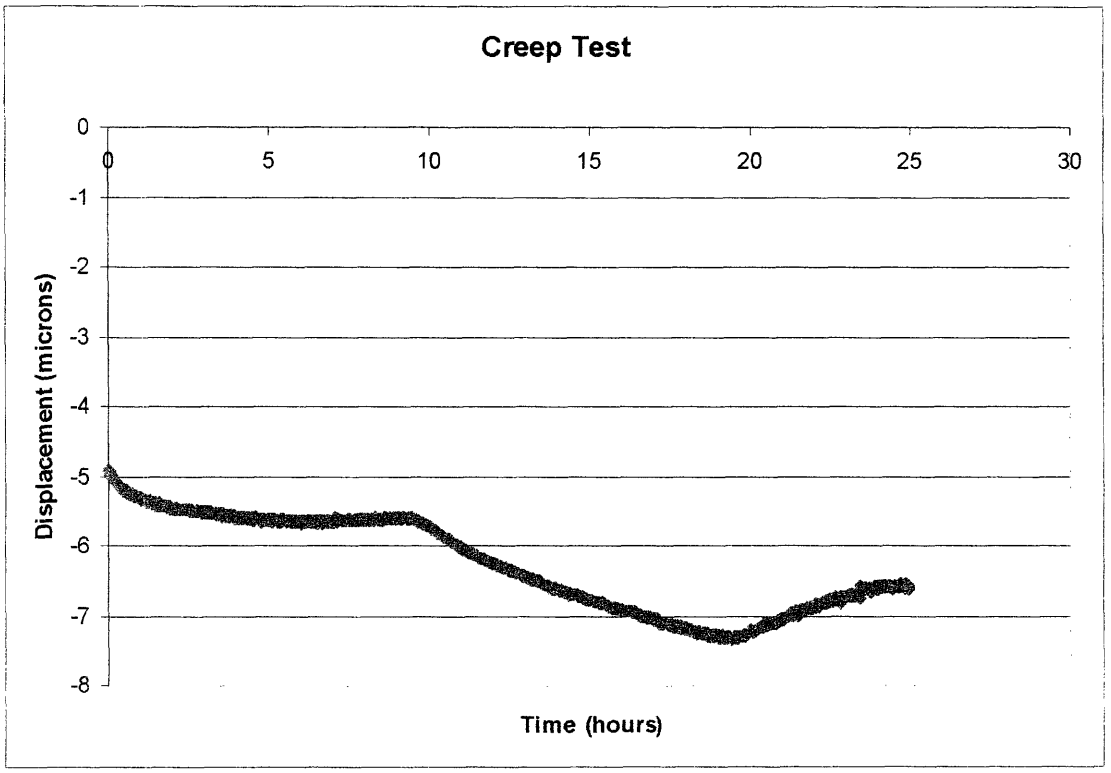

Figure 35: Results of the Creep Test

Here too, thermal fluctuations cause fluctuations in displacement, but the overall trend is downward. As discussed above, this means the stage is rising, and for a loading in the negative z direction as shown in Figure 24, this is to be expected. It is clear that 24 hours are not enough to fully investigate the effects.

6.0 Conclusion and Discussion

This research achieved its main goals: a plastically deformed monolithic compliant Nanomanipulator was designed and fabricated successfully. It correlated very well to FEA data, and showed only small indications of hysteresis. Further tests investigated the visco-elastic properties of the mechanism, and all showed that if the mechanism does vary in time, the

variation is on the order of hours. Modern control systems make many corrections each second, so this should not be a problem. The post-forming test showed a position drift of 6-7 microns over the course of the day following the formation of the mechanism, and creep effects were somewhere on the order of 2 microns over the course of 24 hours of continuous near-yield loading. This corresponds to an average velocity of .02 nanometers per second. In comparison, piezo actuators can achieve a velocity of 2×10^8 nanometers per second. In addition, given that the range of the mechanism is on the order of 75 microns, this is hardly significant. However, if it does become significant, it is easy enough to correct for these problems. To avoid post-processing effects, the user could wait a few days between the fabrication of the part and the actual use. In fact, in most applications, between shipping, storage, integration, and transport, it is likely that the visco-elastic effects would have subsided by the time it is actually used. To correct for creep, it is wise not to load the mechanism continuously. If there is a situation where continuous load is required, the equilibrium position should be shifted to compensate.

Possible directions for further work might include:

- Experimentation with different materials that perform better in the forming process. A careful review of the desirable properties would also be in order.
- Reconfiguration of the mechanism to be actuated with electro-magnetic actuators as was done with the HexFlex, not just micrometer heads.
- A more thorough investigation of the effects of defects induced by the waterjet, as well as ways to minimize both the defects and the negative effects they cause.
- Construction of a forming machine to introduce repeatability and accuracy into the pressing process. Indeed, at the time of writing, work is being done to design and fabricate a hydro-pneumatic press with force and position sensing, capable of applying up to 2.5 tons of force with

accuracy on the order of several thousandths of an inch. It will be run off a compressed air source, and will be actuated by a computer-controlled solenoid. Hopefully, using this new machinery, further accuracy can be introduced into the process.

- Observation of similar tests while also taking readings from a thermocouple, to further attempt to extract out the effects of temperature.

- Further experimentation, specifically in the areas of fatigue (effects of cyclic loading) and creep (longer duration, increased load) to better understand the mechanisms behind both.

To restate: the prototype 3D Nanomanipulator that was constructed had good correlation to predicted results, and was not unruly in its behavior. Thus, it is possible to conclude that plastic deformation can indeed be successfully integrated into precision compliant mechanism design in the area of nanomanipulation, and, if care is taken in the implementation, in other areas as well.

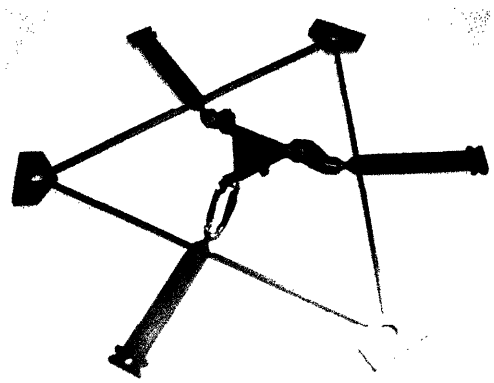

7.0 References

[1] Anderson, G. A., 2003. A Six Degree of Freedom Flexural Positioning Stage. SM Thesis, Massachusetts Institute of Technology, Cambridge, MA.

[2] Goedertier, P. V., "Unitary Q-switch laser device," US Pat. No. 3,500,234, 1966.

[3] Heyler, R., "Package design considerations for automated assembly," www.newport.com/support/magazine_features/fpn01.asp

[4] Howell, L. L., 2001. Compliant Mechanisms. John Wiley and Sons, New York.

[5] Jang, S., Heyler, R., "Process for detecting and correcting a misalignment between a fiber cable and a light source within a fiber module," US Pat. No. 6,184,987B1, 2001.

[6] Kalpakjian, S., and Schmid, S. R., 2001. Manufacturing Engineering and Technology. 4th ed. Prentice-Hall, Upper Saddle River, NJ.

[7] Katagiri, T., Tachikura, M., Murakami, Y., "Basic design for stable fiber clamping in multi-fiber ribbon mechanical splice," IEICE Transactions of Communication, vol. E84-B, No. 8, pp. 2161-69 August 2001.

[8] Kindl, H., Westermeier, H., "Gas Laser," US Pat. No. 3.826,998, 1974.

[9] Knowles, K. H., "Laser components and fabrication method," US Pat. No. 3,978,425, 1976.

[10] Masghati, M., Racz, L. M., "Re-entrant alignment features for optical components," US Pat. Application. No. US2002/0048446A1, 2002.

[11] Pan, J., Jiang, P. S., Shih, M., Chen, J., Wang, L., "Fiber optic support clip," US Pat. No. 5,619,609, 1997.

[12] Shimaoka, M., Kumazawa, T., Yagiu, Y., Sasayama, A., "Optical coupling apparatus and manufacturing of the same and lens holder," US Pat. No. 5,195,155, 1993.

[13] Slocum, A. H., 1992. Precision Machine Design. Society of Manufacturing Engineers, Dearborn, MI.

[14] Van den Brink, H. G., Van Hoof, A. J. F. M., Van Kleef, J. H. K. C., Lamboo, T. F., "A method of adjusting gas laser mirror," US Pat. No. 4,217,559, 1980.

[15] Verviell, J., "Optical electronic assembly having a flexure for maintaining alignment between optical elements," US Pat. 6,207,950B1, 2001.

[16] Verviell, J., "Opto-electronic assembly and method of making the same," US Pat. No. 5,977,567, 1999.

Appendix A: Full Data from Input/Output Correlation Tests

Sam Korb
January 6, 2004
PSDAM

Test 1: Input: In Plane, Two points of Equal and Opposite Actuation
Output: One-dimensional (Y) Translation In Plane

Actuators: Micrometer Heads
Sensor: Dial Gauge on the side of the stage, normal to the Y direction

FEA Deflection of Micrometer Heads at Yield Stress:	0.0004714 meters	0.0185591 in
Resultant Deflection of Stage at that Value:	0.0001496 meters	0.0058898 in
Transmission ratio:	3.151069519	
Maximum Test Deflection: Deflection at Yield/2:	0.0002357 meters	0.0092795 in

Experimental Data:

Point	Input (in)		Output (in) Ascent	Output (in) Descent		Expected
0	0.0000		0.0000	0.0001		0.0000
1	0.0009		0.0003	0.0005		0.0003
2	0.0019		0.0007	0.0007		0.0006
3	0.0028		0.001	0.001		0.0009
4	0.0037		0.0013	0.0014		0.0012
5	0.0046		0.0015	0.0016		0.0015
6	0.0056		0.0018	0.002		0.0018
7	0.0065		0.0021	0.0022		0.0021
8	0.0074		0.0025	0.0026		0.0024
9	0.0084		0.0027	0.0029		0.0027
10	0.0093		0.003	0.003		0.0029

Sam Korb
January 6, 2004
PSDAM

Test 2: Input: Out of Plane, Three points of Equal Actuation
Output: One-Dimensional (Z) Translation Out of Plane

Actuators: Micrometer Heads
Sensor: Dial Gauge on the top of the stage, normal to the Z direction

FEA Deflection of Micrometer Heads at Yield Stress:	0.0008848 meters	0.0348346 in
Resultant Deflection of Stage at that Value:	7.84E-05 meters	0.0030878 in
Transmission ratio:	11.28139742	
Maximum Test Deflection: Deflection at Yield/2:	0.0004424 meters	0.0174173 in

Experimental Data:

Point	Input (in)		Output (in) Ascent	Output (in) Descent		Expected Output (in)
0	0.0000		0	0		0.0000
1	0.0017		0.0002	0.0002		0.0002
2	0.0035		0.0003	0.0004		0.0003
3	0.0052		0.0005	0.0005		0.0005
4	0.0070		0.0007	0.0007		0.0006
5	0.0087		0.0008	0.001		0.0008
6	0.0105		0.0011	0.0011		0.0009
7	0.0122		0.0012	0.0012		0.0011
8	0.0139		0.0014	0.0015		0.0012
9	0.0157		0.0016	0.0017		0.0014
10	0.0174		0.0018	0.0018		0.0015

Sam Korb January 19, 2004 PSDAM

Test 3: Input: In-Plane, Three points of Equal Actuation
Output: In-Plane Rotation about Z Axis
Actuators: Micrometer Heads
Sensor: Dial Gauge sensing displacement of an output-amplifying cantilever attached to the stage

FEA Deflection of Micrometer Heads at Yield Stress:	0.000211817	meters	0.0083393 in
Resultant Deflection of Test Point at that Value:	1.03E-05	meters	0.0004063 in
Distance of Actuation Point from Center of Rotation			2 in
Distance of Test Point from Center of Mechanism:			0.415247 in
Angle Deflection at Yield Stress:			0.0009783 radians
Transmission ratio:	4.261906492		
Maximum Test Deflection: Deflection at Yield/2:	0.000105909	meters	0.0041696 in

Experimental Data:

Point	Input (in)		Output (in) Ascent	Output (in) Descent		Expected Output (in)
0	0.0000		0	0.0001		0.0000
1	0.0004		0.0002	0.0002		0.0002
2	0.0008		0.0004	0.0004		0.0005
3	0.0013		0.0006	0.0007		0.0007
4	0.0017		0.0008	0.0009		0.0009
5	0.0021		0.0011	0.0012		0.0012
6	0.0025		0.0013	0.0014		0.0014
7	0.0029		0.0014	0.0016		0.0016
8	0.0033		0.0017	0.0018		0.0019
9	0.0038		0.002	0.0021		0.0021
10	0.0042		0.0022	0.0022		0.0023

Distance of Test Point from Center of Mechanism: 4.763 in

Point	input (radians)	ascending (radians	descending (radians)	expected (radians)
0	0.00000	0.00000	0.00002	0.00000
1	0.00021	0.00004	0.00004	0.00005
2	0.00042	0.00008	0.00008	0.00010
3	0.00063	0.00013	0.00015	0.00015
4	0.00083	0.00017	0.00019	0.00020
5	0.00104	0.00023	0.00025	0.00024
6	0.00125	0.00027	0.00029	0.00029
7	0.00146	0.00029	0.00034	0.00034
8	0.00167	0.00036	0.00038	0.00039
9	0.00188	0.00042	0.00044	0.00044
10	0.00208	0.00046	0.00046	0.00049

Appendix B: COSMOSWorks Stress/Strain Plots of the Tests

Test 1: In Plane, Two points of Equal and Opposite Actuation

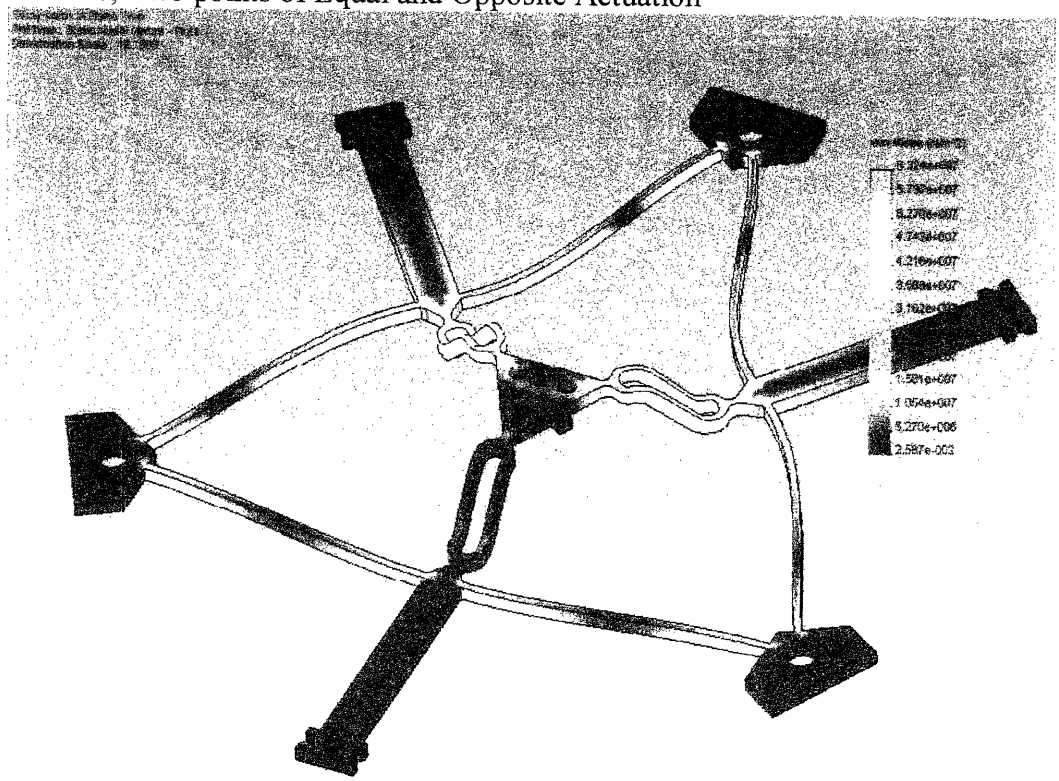

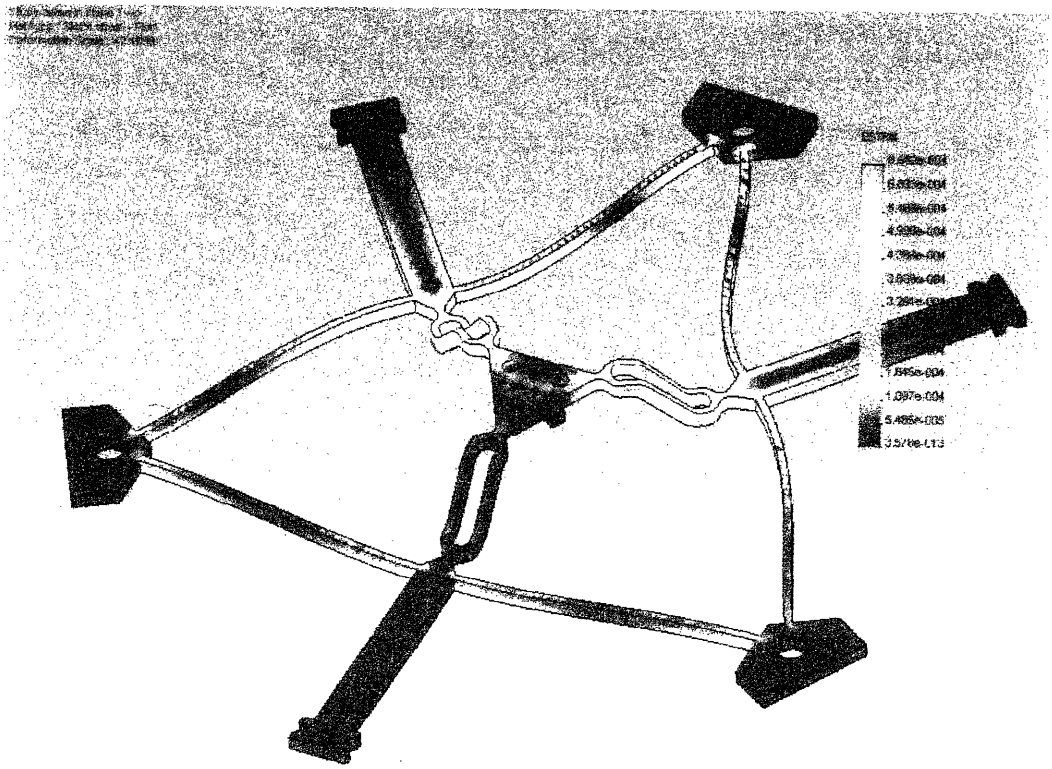

Test 2: In Plane, Three points of Equal Actuation

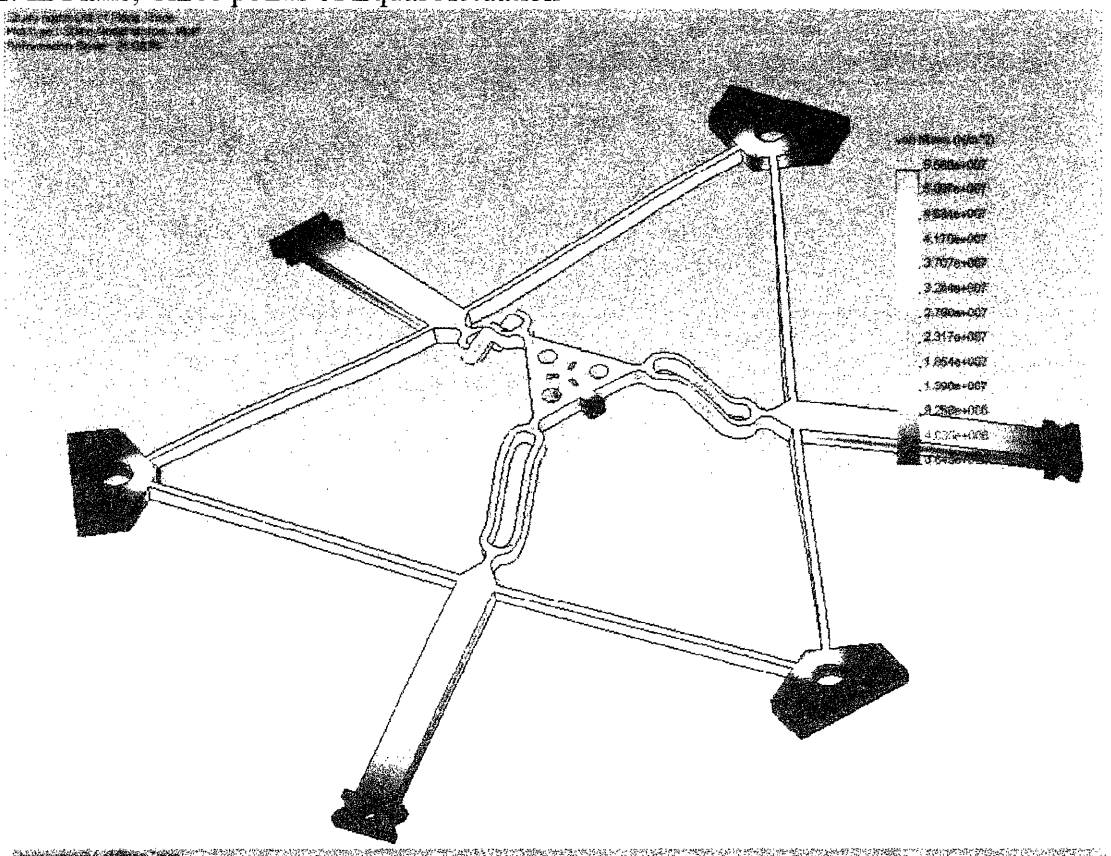

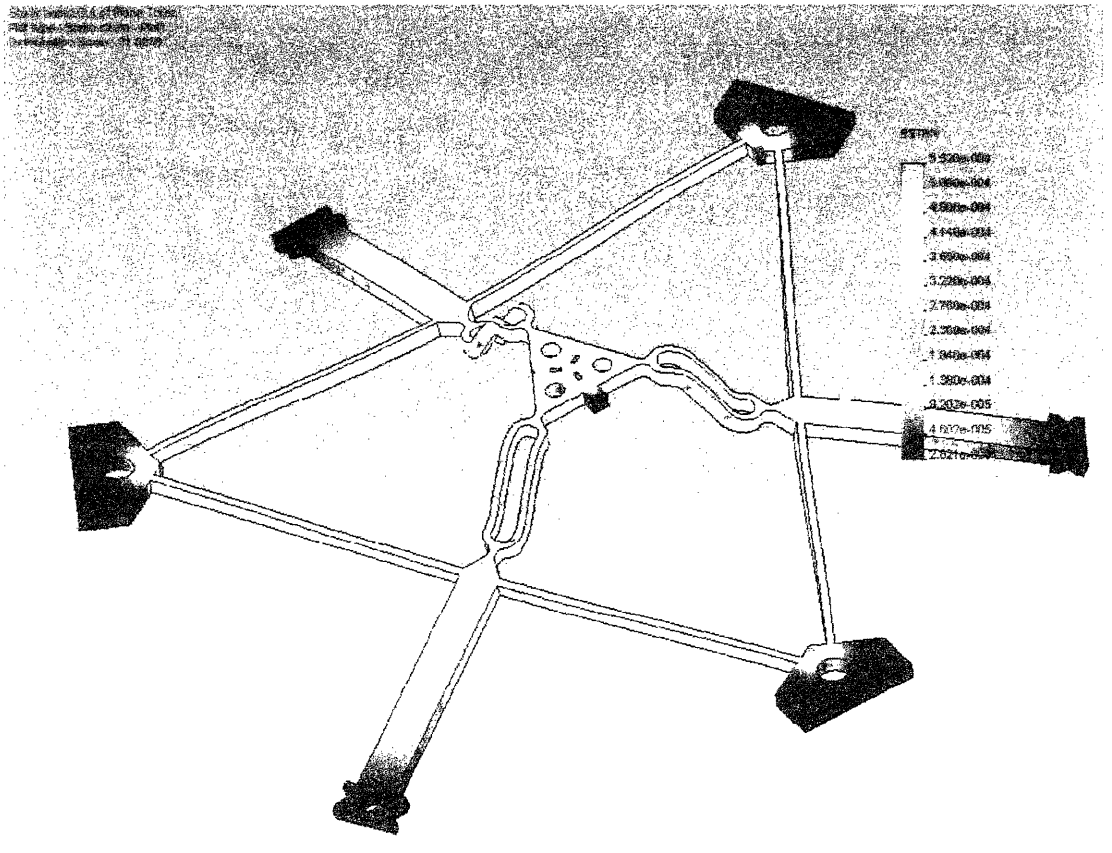

Test Three: Out of Plane, Three points of Equal Actuation